NTNU

Norwegian University of
Science and Technology

Control of wireless power transfer systems for marine applications

Lars Jakob Paulsen

Master of Science in Electric Power Engineering
Submission date: June 2016
Supervisor: Elisabetta Tedeschi, ELKRAFT
Co-supervisor: Giuseppe Guidi, SINTEF Energy Research

Norwegian University of Science and Technology
Department of Electric Power Engineering

Problem description

Wireless power transfer is the technology to transfer power without any conductors touching. The type of wireless power transfer that is most commonly researched is to use magnetically coupled inductors. This technology is called Inductive power transfer, and it provides a good and stable connection as long as the coils are relatively close to each other and correctly aligned. For marine applications the coils are moving, which makes it crucial to have a good control system to control the power flow and output voltage and currents.

This master thesis will investigate the requirements, operation and performance of control techniques for wireless charging in marine applications. This will be done by using simulation tools to study the magnetic coupling as the coupling is changed by movement of the coils. The inductive power system must have a controller which can handle the changes and be able to control the output to fit the application. Marine and offshore applications tend to have large power ratings, which introduce some new challenges. The Matlab/Simulink environment will be used for such analyses. Initially the model from the specialization project will be further developed, and then a controller can be tested and designed using Matlab/Simulink.

Abstract

This report is a master thesis whose purpose is to show the steps in designing a control system used for regulating a system for inductive power transfer (IPT) of marine vessel and offshore applications.

The constant increase in focus on green energy and CO_2-emission reductions has led to an increase in electrification. Especially electrification of the transportation sector has great impact on the global CO_2-emissions, thus the amount of vehicles and marine vessels that runs on electricity has increased rapidly and still is. This is where wireless power transfer (WPT) will be an important technology. Wireless power transfer refers to the art of transferring power without the need of physical contact. In this thesis only "*inductive power transfer*" (IPT) will be covered, because it is the most promising technology for charging vehicles and providing large power transfer to vessels or offshore applications. "*Inductive power transfer*" is in principle a coreless transformer that transfers power via the induced magnetic field created by the coil on the sending side that induces currents in the coil on the load side. This technology has several perks compared to cables, such as: increased safety, easy to connect, minimizes the need for maintenance of the power supply and it is well suited for rough environments.

During the autumn 2015, some models of a basic IPT-system were made, and measurements of a working IPT prototype were done. The prototype was part of a SINTEF project on battery charging marine vessels. This thesis is the continuation of this project, and the objectives are to upgrade the average, nonlinear time-invariant model found in the project work and then linearize it. The linearized model is then analyzed for six different cases where the coupling coefficient is changed and the respective transfer functions are extracted. The transfer functions are analyzed with respect to control theory, and the possibility of second order approximations are tested. Finally the design procedure of an initial controller for the IPT system is done by the use of MatLab/Simulink.

The results from the analysis of the transfer functions shows that the transfer functions have valid second order approximations at low coupling coefficients, but as the coupling gets stronger (coils are separated by a smaller air gap) the approximation becomes invalid. The second order design methods provide the best tools for handling design of a controller, but because systems may not always be represented by a second order approximations in its operation range, Other methods should be explored. For the area that cannot be approximated, design using computer tools are proposed. The theory behind the computer tools should be further studied in order to more easily design controllers that can adapt to changes in the system transfer function according to the coupling of the coils.

For further work I propose to look more into the second order approximation to be able to represent more transfer functions as second order approximations. Additionally, the relationship between the coupling coefficient and how the poles and zeroes are located should be looked into. The mathematical model, based on coupled mode theory, used to model the IPT-system should be further developed.

Sammendrag

Denne rapporten er en avsluttende masteroppgave ment for å vise veien til å designe et kontrollsystem for et induktivt kraftoverføringssystem for marine fartøy og offshore utstyr.

Den konstante økningen av fokus på miljø, fornybar energi og reduksjon av CO_2-utslipp har ført til økt elektrifisering. Spesielt stor er elektrifiseringen av transportsektoren siden den står for mye av de globale $CO2_2$-utslippene. Elektriske biler og marine fartøy som går på bare strøm har økt betydelig, og fortsetter å øke. Dette et marked der trådløs kraftoverføring vil være en viktig teknologi å satse på. Trådløs kraftoverføring refererer til kunsten å overføre strøm uten å trenge fysisk kontakt. I denne oppgaven vil bare «*induktiv kraftoverføring*» bli dekket, fordi det er den mest lovende teknologien for å kunne lade elektriske kjøretøy og for å kunne overføre de store mengdene kraft som trengs for å drive marine fartøy og elektrisk utstyr offshore. Et induktivt kraftoverføringssystem er i prinsippet en kjerneløs transformator som overfører strøm via magnetfeltet som dannes rundt spolen på kraftkilden sin side, og tas opp av den andre spolen på lastsiden. Denne teknologien har flere fordeler ovenfor kabler, som f. eks: økt sikkerhet, lett å tilkoble, minimaliserer behovet for vedlikehold og er veldig robust og tåler tøffe værforhold.

Gjennom høsten 2015, ble modeller av et grunnleggende «*induktivt overføringssystem*» laget og flere målinger av en fungerende prototype ble gjort. Prototypen var en del av et SINTEF prosjekt som omhandlet batterilading av ferger med et «*induktivt overføringssystem*». Denne oppgaven er en fortsettelse på dette prosjektet, og målene er som følger: Å oppgradere den ulineære, tidsuavhengige gjennomsnittsmodellen av systemet og deretter linearisere det. Den lineariserte modellen blir deretter testet for seks caser som simulerer endring i koblingen til spolene avstanden mellom dem endres, og transfer funksjonen kan trekkes ut ved hjelp av MatLab. Transfer-funksjonene blir analysert med vanlig reguleringsteknikk, og det er ønskelig at disse kan bli representert av andre ordens tilnærminger. Til slutt vises design-prosedyren, og førstegangs-kontroller blir designet i MatLab/Simulink.

Analysen av transferfunksjonene viser at når systemet drives med stort luftgap er andre ordens tilnærming gyldig, men ved mindre luft gap/sterkere kobling ser det ut til at andre ordens tilnærming ikke er gyldig. Designmetoder basert på annengrads tilnærminger gir de beste verktøyene for å designe en kontroller, men det er ikke alltid en andreordens tilnærming er gyldig. Siden noen operasjonstilstander av det «induktive kraftoverføringssystemet» kan gi transferfunksjoner som ikke kan representeres med andreordens tilnærminger, burde andre alternative designmetoder utforskes. Derfor foreslås det å sette seg inn i dataverktøy og designe kontroller ved hjelp av teorien som brukes av programmer som Control System Manager som er en del av Matlab. Dette kan brukes for å designe en kontroller som tilpasser seg endringer av koblingsstyrken til spolene.

For videre arbeid foreslår jeg å utforske annengrads tilnærminger mer, for å kunne representere flere transfer funksjoner godt nok som annengrads tilnærminger. I tillegg, burde forholdet

mellom lokasjonen til poler/nullpunkter med koblingskoeffisienten til spolene. Modellen som er blitt brukt til å beskrive «induktiv kraftoverføringssystemet», bør utvides og undersøkes mer.

Acknowledgements

This project was carried out at the Department of Electric Power Engineering of the Norwegian University of Technology (NTNU) under the co-supervision of SINTEF Energy Research.

First, I would like to sincerely express my gratitude to my supervisor at NTNU, prof. Elisabetta Tedeschi, Department of Electric Power Engineering, for her guidance, helpful feedback and quick response to emails during the execution of this project.

In addition, I want to thank my co-supervisor research scientist Giuseppe Guidi from SINTEF Energy Research, for giving helpful advice on the technical aspects of the project.
I would also like to thank my family, who has supported me through the whole process

My friends and colleagues have also helped me through the process with their helpful and encouraging comments.

Table of contents

List of figures

List of tables

1 Introduction

Electricity is the most important infrastructure in the modern world. Almost every part of our daily life demands electricity. Traditionally, electricity is produced by huge centralized power plants burning fossil fuel. But today, the focus gets more shifted towards CO_2-emission reductions and towards increasing the percentage of energy created by renewable energy sources. By phasing out the electricity production based on fossil fuel, electricity becomes more attractive as the main energy medium for all sectors. It is a consensus that reduction of climate gases and increase in renewable energy is the first step in the right direction to a sustainable energy production. Especially the transport sector has great potential when it comes to reducing the usage of fossil fuels, either by using hybrid systems or fully electrical propulsion.

As the focus on electricity increases, more research is focused on making the electrification of the transport and marine sector possible. This will require large power transfers, which presents some security hazards when using conventional cables and sockets to "plug" the application to the power source for charging. This is where wireless power transfer (WPT) introduces new possibilities that increase safety and facilitate the establishment of the power transfer.

Wireless power transfer is a general term for transferring power without the need of physical contact, but in this thesis the focus will be solely on inductive power transfer (IPT). To further explain the concept of inductive charging, an electrical vehicle (EV) is shown in Figure 1.1 where an adapter is mounted on the vehicle.

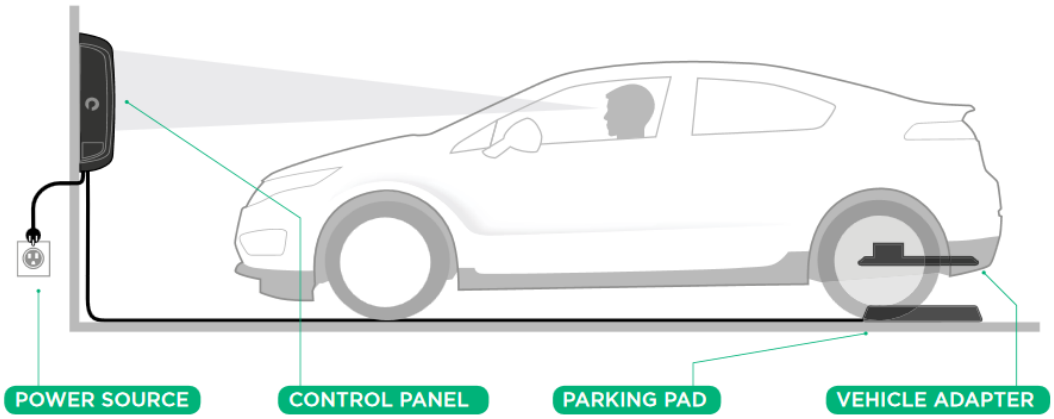

Figure 1.1 shows how Plugless offers electrical vehicle customers to charge their cars wirelessly[1].

This adapter is connected to the car's electrical system and the parking pad is connected to the grid. The power transfer is possible because both the pad and the mounted adapter each contain a

coil that is magnetically coupled to the other. This means that current running through the coil in the parking pad creates a varying magnetic field that induces currents in the receiving coil of the adapter. The car needs to be parked in the correct spot and it charges automatically. This technology has also been introduced to consumer products like cell phones, cameras and other electronics with batteries.

It is quite simple to design IPT-systems for stationary applications like a parked car or consumer electronics as the coupling between the coils are constant. Even though it seems simple in theory, many factors need to be taken into account when designing an IPT-system. Changes in the load and changes in the coupling are the most typical challenges that may change both power transfer capacity and the voltage and current magnitudes to the load. In order to cope with these challenges, both the design of the components and the control system are important. In this thesis the main focus is on control design.

Wireless power transfer saves time and reduces wear and tear compared to traditional solutions. Another promising use of wireless power transfer is in bio-implants that typically have a battery pack. Earlier, the patient needed to have another surgery to replace the batteries, or even worse, have an external power source and wires through the tissue to power the implant. Inductive power transfer (IPT) allows the external power source to simply be placed in the vicinity of the implant to power it.

1.1 Background for WPT

The physics behind wireless power transfer is based on both Maxwell's equations that were postulated in 1862, and on Ampere's and Faraday's work. Ampere's circuit law describes how the current and the electric field in a conductor are proportional to the magnetic field circulating the cross section of the conductor. Faraday's law of induction describes how changes in the magnetic field around a circuit induce an electromotive force (emf). These laws were the foundation of the field of electrical engineering, and since that time scientists have searched for a way to transfer power without the need of wires. Faraday made direct current (dc) machines and alternating current (ac) machines possible, and Nikola Tesla greatly improved these when he invented the induction machine[2]. Wireless power transfer does happen between the stator and rotor of the induction machine, but the coupling distance is very short and contained. Nikola Tesla was a genius when it came to electrical engineering and he dedicated his life to exploring the phenomenon electricity and its limits. Especially the thought of wireless power transfer intrigued him[3]. Tesla did several experiments on wireless power transfer by using the famous tesla coils, but they were neither reliable, efficient nor safe for practical applications. The failed experiments on wireless power in the late 19^{th} century led to a breakthrough in sending information wirelessly, but for almost a century wireless power transfer seemed like an unreachable dream. During the 1800's and most of the 1900's there were huge discoveries made on long distance communication, but nothing happened on the wireless power transfer front.

WPT began to fetch academic interest in the late 1970's in the field of powering electrical vehicles[2]. In the 1980's a huge project on IPT-driven vehicles was conducted by The Partner for Advanced Transit and Highways and called the PATH-project. This project was done in California and developed a roadway powered IPT vehicle with a variable air gap[4]. They managed to couple a bus using IPT and achieving 60% efficiency at a controlled gap of 50-100mm. The tests showed that up to 40 kW could be transferred if the bus battery was totally discharged[4]. The gap was increased to 150-200mm when power transfer was not needed. This system used capacitive detuning of the pickup system to control the power. This demanded huge amounts of reactive power from the generator, which was possible, but at reduced efficiency. The PATH project was later abandoned due to higher costs and more losses than anticipated.

With the rapid development of new and better power electronics, the WPT industry has grown from a technological curiosity in 1995 to the billion-dollar industry it is today. Close to the millennia shift huge progress has been made on WPT of short gap and stable coupling applications. After gaining full understanding of stationary IPT-systems, the research has been focused on handling changes in parameters like coupling and load. Research on new ways to model IPT-systems, and research on control systems governing the power transfer and voltages and currents to ensure desired operation has increased a lot in the last decade[2]. This research is important to be able to: optimize bio-implants, and to charge offshore applications and electric powered vessels while waves move the pickup adapter relative to the power source.

1.2 WPT today and in the future

The huge increase in research on wireless power transfer and the capabilities of today's power electronics have made it possible to make working prototypes for the transport sector. The Plugless pad shown in the introduction is one example of a working prototype that the customers appreciate. Another new prototype that is very relevant to this thesis is made by the marine company Wärtsilä, which focuses on new energy solutions for the marine sector. They have designed a prototype of a wireless charging station for marine vessels that also works as the mooring[5]. This can make not only the charging of battery ferries easier, but also eliminate the need for many huge and cumbersome cables when providing ships in port electricity (cold ironing). Medical implants have also greatly improved as wireless power transfer has been developed. Implants can now be powered deep into the body from the outside without harmful wires through tissue[6]. Research on medical micro robots, that is powered and controlled by a WPT connection, is also a field of research[7]. The main barrier for a huge WPT revolution today is the difference in cost and the reduced efficiency compared to traditional solutions[8]. But the costs are being reduced, and a lot of research on maximum power tracking is done[9].

In the future, WPT-systems will enable power to be transferred wirelessly at acceptable efficiencies everywhere within a set domain. One such domain may be apartments, mono rails and other railway systems, or the roads themselves may power the cars. This will enable great

reduction in the needed battery capacity of appliances or even remove the need for batteries for some[6]. Especially the transport sector will benefit greatly from this since the batteries in EV represent the majority of the weight of the vehicle. The greatest challenge is to implement WPT in a cost efficient way. However, great improvements of the technology are made every year.

1.3 Objectives

During autumn 2015, the specialization project that this thesis is an extension of was done. There, mathematical models and simulations for a simple IPT-system were developed, which needed to be further tested. The first objective of this thesis is to improve the mathematical models and the simulations to be good approximations of the real system. When the models are updated, the next objective is to make a linear approximation of the system to facilitate the design of a control system. When the linearization is performed and the desired transfer function is extracted, the final objective can be fulfilled. The final objective is to design a controller for a simple IPT-system by the use of classic control theory. As a side objective, the possibilities and challenges of wireless power transfer will be considered and discussed.

1.4 Limitations

This thesis will only cover the basic topologies of IPT-systems, where the power electronics are modeled as voltage sources, and the circuit is described by simple resistors, inductors and capacitors. There are also other ways to transfer power wirelessly, but for this thesis inductive power transfer is chosen. Also, in order to get manageable results, the nonlinear system needs to be linearized and only basic linear control theory will be used to analyze and design the controller. For the design of the controller, a certain interval of different strengths of the magnetic coupling between the coils will be analyzed, and only linear movement of the coil will be considered. That means that the rotation of coils during operation is considered small enough to be neglected for marine and offshore applications. Available papers focusing on marine and offshore applications are scarce, but most traits and phenomena regarding IPT-systems are the same for all IPT applications.

1.5 Approach

The first objective will be achieved by testing the response from several successive changes in the input, unlike the single step change in the earlier project. The linearization of the nonlinear, time-invariant averaged model, is done according to the steps done by Hongchang et al.[10]. First, linearize the system using state space model (time domain), then transform it to frequency domain (see chapter 4.3 for details). The design of the controller is done in several steps: first, the linearized transfer function needs to be checked for the system settings giving the best coupling between the coil, then the lowest acceptable coupling. Individually, these settings give quite different transfer functions and responses. The two different transfer functions need to be

simplified, preferably from a fourth order system to a second order approximation of the system. Then, a controller is designed in frequency domain using Bode plots and basic control theory procedure. The additional objective is reached by reading recent research on WPT-systems and cross reference introductions from several papers.

1.6 Structure of report

In chapter 2, the basics for an inductive power transfer is explained and the most important components are shown. This includes the magnetically coupled coils, the effects of changes in the relative positioning of the coils, and why the coupled coils need capacitive compensation. Finally, a working IPT-system is explained. To be able to work and analyze an IPT-system, we need to make mathematical models.

Chapter 3 explains how the different models have been derived, what they are used for, and the needed simulations of a basic IPT-system is shown. The default parameters will be defined and comparisons between models will help verify the validity of the model, which will be used for further studies.

Chapter 4 is all about control theory used to analyze the IPT-system. The chapter starts with, introducing both modelling in frequency domain and time domain, and making a short comparison of the two methods. Followed by theory and expressions used to linearize the nonlinear averaged model. After the process of linearization is explained, second order systems are explained. Theory used to make a second order approximation of the higher order IPT-system is also explained, and important design criteria are explained with respect to the IPT-system and second order approximations. This chapter is concluded with, some theory on controllers/compensators to optimize the IPT-system will be given.

Chapter 5 will use the theory explained in chapter 4 on six different cases to simulate the effect of coil misalignment. The six cases will be modelled, then linearized using MatLab and finally analyzed. The results will be shown for each step on the way accompanied by important discoveries.

Chapter 6 discusses the design of a controller using computer tools

2 System theory for an inductive power transfer system

An inductive power transfer system is one way to transfer power from a power source to an application without the need of physical connection of conductors. This chapter will explain the theory behind the IPT-system and highlight its important components. An understanding of how the physical system and its components behave is important in order to design appropriate control systems.

2.1 Mutually coupled magnetic circuit

The heart of an inductive power transfer system is the magnetic link formed between the two circuits. The circuit for the power source is mutually coupled to the circuit of the application that needs power. This thesis will only handle two circuit systems with one sending side and one receiving side. Current running in the primary side induces a voltage in the secondary circuit as is indicated in Figure 2.1. There will only be a current present in the secondary circuit if there is a load present.

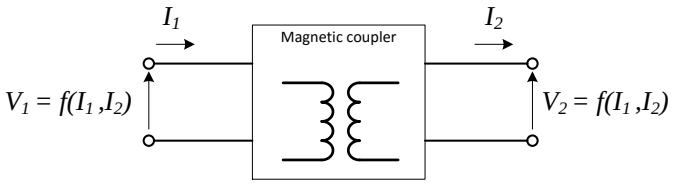

Figure 2.1 shows two magnetically coupled circuits[11].

With the scope limited to only two circuits, the magnetic coupling also known as inductive coupling can be described by the following three parameters:

L_{11} : Self Inductance of Coil 1;

L_{22} : Self Inductance of Coil 2;

M : Mutual Inductance between Coil 1 and Coil 2.

The most known application of inductive coupling is found in a standard transformer, where the magnetic coupling is enhanced by having an iron core to properly guide the flux. For contactless power transfer applications, the typical medium between the sending coil and the receiving coil will be high reluctance materials such as air, water and all sorts of protective plastic materials. A

coefficient that describes the strength of the inductive coupling between two coils is called "*coupling coefficient*" and is defined as:

$$k = \frac{M}{\sqrt{L_{11} \cdot L_{22}}} \tag{2.1}$$

From energy conservation it can be shown that this coefficient has to be in the range from zero to unity[11], where a coupling coefficient of zero means no coupling at all, and unity means ideal coupling with no leakage flux (ideal transformer). Mutually coupled circuits can typically be represented by an equivalent based on the relationship between the currents and voltages of the coupled circuits, or an ideal transformer equivalent. Equation (2.2) shows the relationship of the voltages and currents as functions of the self-inductances and mutual inductance.

$$\begin{aligned} V_1 &= j\omega L_{11} \cdot I_1 - j\omega M \cdot I_2 \\ V_2 &= j\omega L_{22} \cdot I_2 + j\omega M \cdot I_1 \end{aligned} \tag{2.2}$$

These equations describe the equivalent representation shown in Figure 2.2 a) where the contribution from the mutual inductance can be modeled as voltage sources. This representation is advantageous in some situations, but the ideal transformer equivalent has advantages that makes it more used. The transformer equivalent combines the two circuits into one circuit, which is more intuitive to work with. Additionally, the physical number of turns can be described in this model if necessary.

a) Based on coupling equations

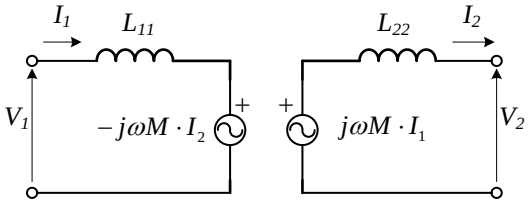

b) Ideal transformer equivalent

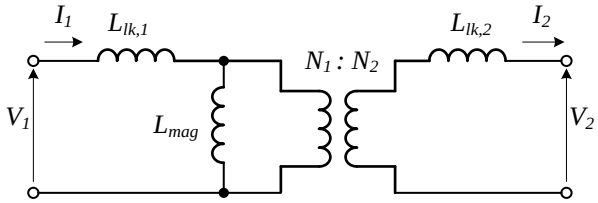

Figure 2.2 shows two equivalent representations of mutually coupled circuits[11].

The relationship between the two equivalents are given in equation (2.3), given that the currents and voltages at both coil terminals are equal[11].

$$\begin{aligned} L_{mag} &= M \cdot \frac{N_1}{N_2} = \frac{M}{n} \\ L_{lk1} &= L_{11} - L_{mag} \\ L_{lk2} &= L_{22} - n^2 \cdot L_{mag} \end{aligned} \tag{2.3}$$

In eq.(2.3), L_{lkn} is the leakage inductance at coil 1 or 2 depending on subscript, and N_1 and N_2 refer to the number of turns on coil 1 and coil 2 respectively. Notice how n is defined as N_2:N_1, which is often used when handling transformer equivalents.

2.1.1 Power transfer efficiency for two mutually coupled circuits

Another important parameter concerning inductive power transfer is the quality factor of the coils. The quality factor (Q) can be defined as the ratio of energy stored (E_{Li}) in the circuit reactance related to the power dissipated ($P_{Loss,i}$) in the equivalent resistance of the coil ($R_{ac,i}$)[12]. The angular frequency of operation (ω_o) is important for the resulting quality-factor of a coil.

$$Q = \sqrt{Q_1 Q_2}; \quad Q_i = \frac{\omega_o E_{Li}}{P_{Loss,i}} \approx \frac{\omega_o L_i}{R_{ac,i}} \tag{2.4}$$

As shown in the book about inductive powering[13], the efficiency of mutually coupled coils can be expressed as a function of the quality factor (Q) and the coupling coefficient (k):

$$\eta_{\max} = \frac{(k \cdot Q)^2}{\left(1 + \sqrt{1 + (k \cdot Q)^2}\right)^2} \approx 1 - \frac{2}{k \cdot Q} \tag{2.5}$$

The approximation is valid when (Q×k) >>1. The quality factor for inductively coupled circuits is the geometric average of the individual quality factors of both the sending and receiving inductor which is shown in eq (2.4).

2.1.2 The effect of coil misalignment

The coupling coefficient defined in eq. (2.1) varies greatly with the relative positions of the sending and pickup coil. In total, there are six different possible misalignments that can be divided into two groups. The first group of misalignment is lateral misalignment, which means distance between coils, horizontal displacement and vertical displacement of the coil(s). The other group is angular misalignment, which means rotation of one or both coils along up to three axes. These misalignment groups are not considered to be strongly correlated[14], which makes it possible to study their effects individually. In this thesis only lateral misalignment will be considered, as the angular misalignment is smaller for larger applications like charging ferries or large offshore applications. In the pre-project of this thesis, several measurements of the changes in the inductances and the coupling coefficient with varying lateral misalignment were conducted[15].

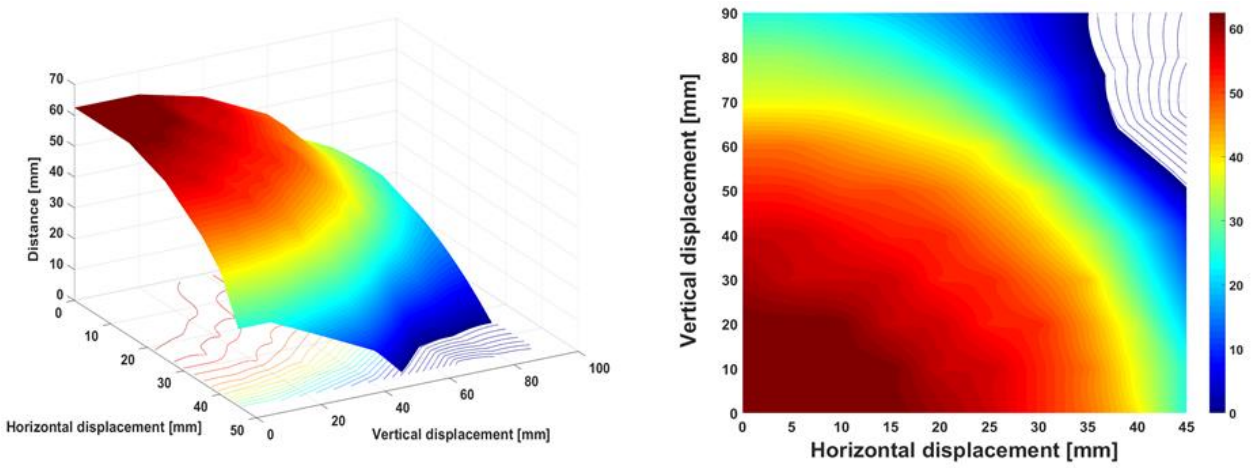

Figure 2.3 shows a surface plot of the effect of misalignment on the coupling coefficient, surface is locked at k=0.185[15].

It is clear from Figure 2.3 that the relative vertical and horizontal position is also important for the coupling coefficient. The effect of lateral misalignment diminishes as the distance between the coils increase [14, 15]. The data used to make the surface plot in Figure 2.3 are taken from a prototype at SINTEF during autumn 2015, and the measurements are shown in Appendix B. The dimensions of the coils used for the measurements are 210mm height by 100mm width. This is important because the change in *k* depends on the misalignment compared to the coil's dimensions, which in turn makes the coil design important for the performance of the IPT-system. Only the coils from the prototype IPT-system at SINTEF will be used along with the measurements done in the specialization project. Coil design and optimization of other components is not considered in this thesis.

These measurements will be used to determine the relevant intervals of the system parameters later in this thesis. The self- inductances of each of the coils as well as the coupling coefficient are the base parameters that define the model. Thus it is important to have measurements of how they change with respect to distance and lateral misalignment.

2.2 Need for capacitive compensation

In chapter 2.1, it is shown that inductively coupled circuits can be represented by a transformer equivalent. An inductive power transfer system is pretty much a coreless transformer, which results in huge leakage inductance compared to conventional transformers. The increased leakage inductance creates problems that have to be compensated for. This is why capacitors are used to reduce and even nullify the effect of the leakage inductance to run the system in resonance. The capacitive compensation is meant to minimize the VA rating of the power source on the primary side, and maximize the power transfer to the secondary side. The ideal operation for both sides is when the power only has a real component, which happens when the capacitive impedance cancels out the inductive impedance from the leakage inductance. Compensation is also a

prerequisite to let the system operate at high efficiency. The compensation may facilitate the operation of the power electronics in zero voltage switching[16].

Another use of the capacitors is to be able to keep the output current or output voltage constant by choosing the compensation topology for each side designed for the application. Usually the compensation is kept simple with either a capacitor in series (S) or in parallel (P) on primary and secondary side, which gives the four possible basic topologies shown in Figure 2.4. The four basic topologies are: S-S, S-P, P-S and P-P where the first and second letter represents primary and secondary side respectively.

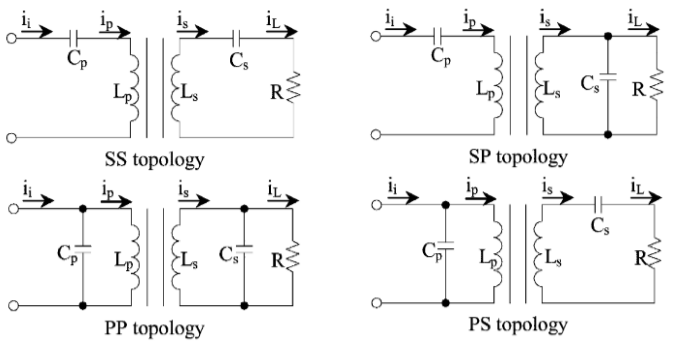

Figure 2.4 shows the four basic compensation topologies[17].

Out of the four basic compensation topologies only the S-S and S-P configurations are considered. That's because the series compensation on primary side is suited for high voltage sources, while parallel compensation suits high current sources. The prototype for an IPT-system at SINTEF has a voltage source in the form of an inverter.

2.2.1 S-S compensation

One of the common topologies is to add capacitors in series on both sides of the air gap to cancel out the self-inductances L_{11} and L_{22} shown in Figure 2.5. The capacitors need to be chosen so that the circuits are run in resonance at the given system frequency *(f_0)*.

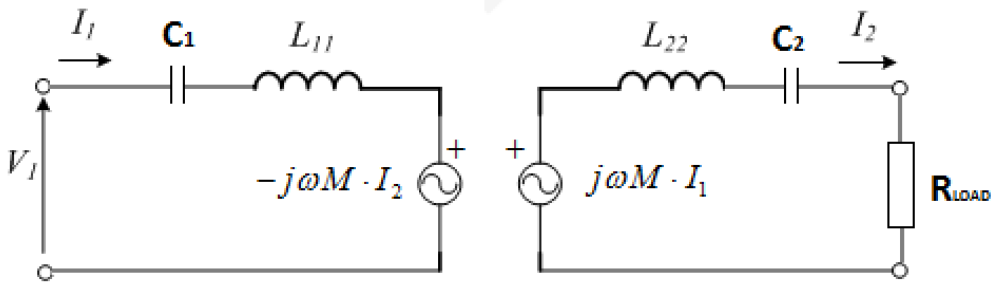

Figure 2.5 shows two mutually coupled circuits that are S-S compensated.

When calculating the required capacitance it is common to calculate the load side capacitor C_2 first. By using complex representation of the impedances on the load side and making sure the imaginary part of the impedance equals zero, the expression for the load side compensation is found:

$$C_2 = \frac{1}{J\omega_0^2 L_{22}} \tag{2.6}$$

The secondary capacitor is easy to calculate for every basic topology, but when calculating the needed capacitance on sending side, another factor needs to be taken into account. In addition to the impedance of the sending side circuit also the reflected impedance of the secondary side seen from the voltage source also needs to be compensated. The mutual coupling shown in Figure 2.5 is based on the coupling equations, which is why the coils are represented by voltage sources. In order to derive an expression for the reflected impedance, simply consider the load side compensated and in resonance and derive the expression for the current I_2. Insert the expression for I_2 into the coupling equation for the primary side and the reflected impedance is found:

$$Z' = -j\omega M \cdot \frac{j\omega M}{R} = \frac{\omega^2 M^2}{R} \tag{2.7}$$

As seen from eq. (2.7) the reflected impedance is purely resistive for an S-S compensated system, which makes the calculation of the primary side capacitance just as simple as when calculating C_2.

$$C_1 = \frac{1}{J\omega_0^2 L_{11}} \tag{2.8}$$

The greatest advantage of the S-S topology is the fact that neither C_1 nor C_2 vary with changes in coupling coefficient nor with varying loading conditions. This ensures that operation in resonance is preserved even as system parameters vary.

2.2.2 S-P compensation

The other basic topology considered in this thesis is the S-P topology, which is shown in Figure 2.6. The procedure to calculate the magnitude of compensation needed is done just as shown for S-S topology.

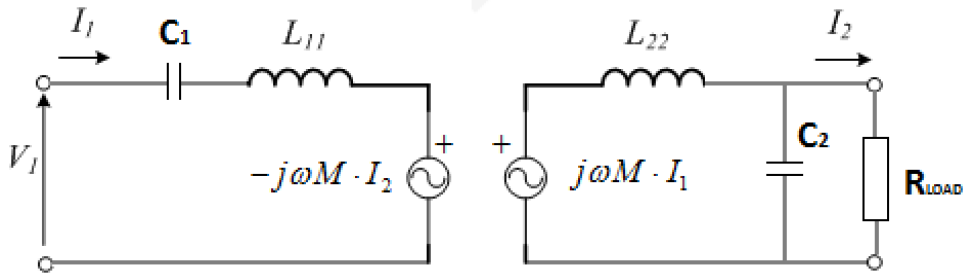

Figure 2.6 shows two mutually coupled circuits that is S-P compensated.

Thus, the load side is to be considered first. Although this time it can be advantageous to make a Norton equivalent of the secondary side to simplify the calculations:

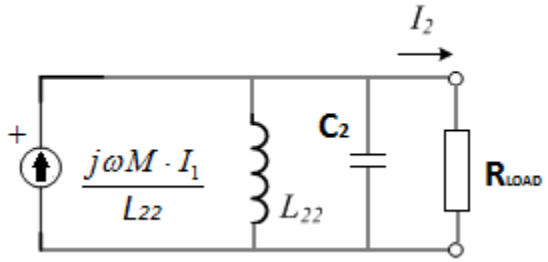

Figure 2.7 shows the Norton equivalent of the load side of the system shown in Figure 2.6.

The system is operated in resonance if the combined impedance of the self-inductance L_{22} and the capacitor C_2 are seen as infinite from the Norton current source. This gives us eq (2.9) that leads to an expression for the load side capacitance in eq (2.10):

$$L_{22}||C_2 = \frac{j\omega L_{22} \cdot \frac{1}{j\omega C_2}}{j\omega L_{22} - \frac{j}{\omega C_2}} \tag{2.9}$$

$$C_2 = \frac{1}{\omega^2 L_{22}} \tag{2.10}$$

The magnitude of capacitive compensation on the load side for S-P topology is the same as found for the S-S topology, but this is not the case for the sending side. To determine the needed compensation on the sending side, the load side current I_2 needs to be inserted in the coupling equation concerning the sending side. Unlike the S-S topology, the reflected impedance now does have an inductive part:

$$Z' = -\frac{j\omega M}{I_1} \cdot \frac{j\omega M I_1}{j\omega L_{22}} = -j\omega \frac{M^2}{L_{22}} \tag{2.11}$$

This means that the compensation on the sending side has to take the inductive reactance into account. The resulting expression for C_1 for S-P topology is:

$$C_1 = \frac{{L_{22}}^2}{\omega^2 L_{22}} \cdot \frac{{L_{22}}^2}{(L_{11}L_{22} - M^2)} = C_2 \cdot \frac{{L_{22}}^2}{(L_{11}L_{22} - M^2)} \tag{2.12}$$

The calculation of C_1 is still quite simple, but since C_1 is now a function of the mutual inductance (M), this topology cannot keep the system in resonance if the coupling changes. In eq. (2.1) it is shown that the coupling coefficient and the mutual inductance are closely related. They both change according to the geometry of the coupled coils, and their positions are relative to each other as described in chapter 2.1.2. The needed capacitances on sending and loading side vary differently according to coupling coefficient, which demands more complex models. To keep the models manageable, the scope of this thesis is thus limited to the S-S topology for capacitive compensation.

2.3 Inductive power transfer system

A working IPT-system needs more components than two coupled coils to work as intended. The currents and voltages going to the load need to be controllable, and the system must be kept in resonance. With the help of Figure 2.8 a simple IPT-system and each component in it will be explained, from the connection to the grid to the connected load.

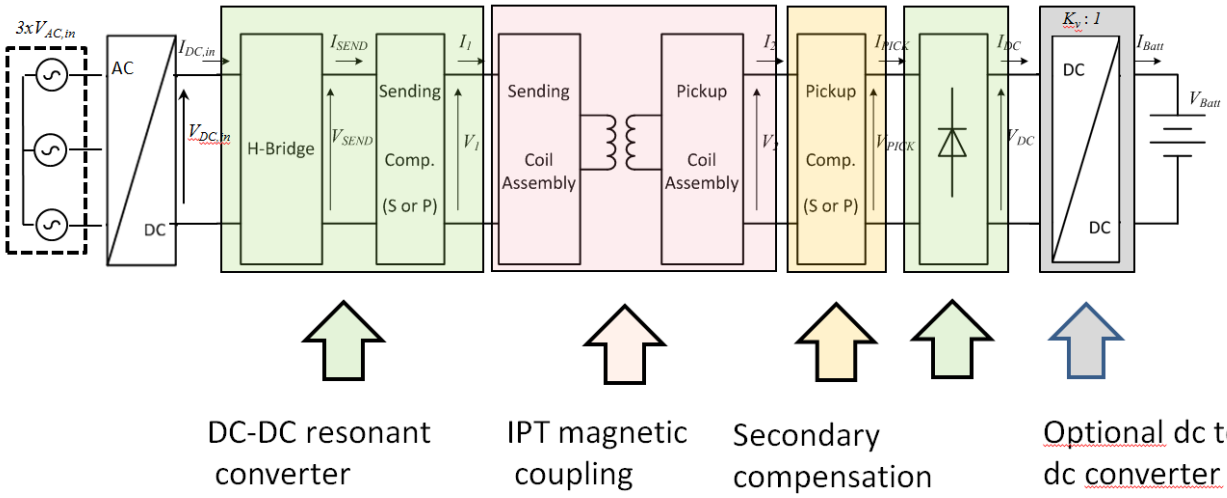

Figure 2.8 shows a block diagram of a battery charging IPT-system connected to the grid with the necessary power electronics[18].

The grid operates at either 50 or 60 Hz, and the connection point may be three phase or single phase. The frequency of the grid needs to be increased to operate an IPT-system efficiently, which is why power electronics are located closest to the grid connection. A rectifier transforms the power from AC to DC in preparation to control the frequency and voltage magnitude going to the coupled inductors. The component responsible for setting the desired frequency and voltage magnitude is the H-bridge inverter. Controllable thyristors or more advanced switching components make sure the input voltage is a square wave that oscillates between V_{DCin} and $-V_{DCin}$ with high frequency. The inverter is a very important component for the control aspect of

this system, as both voltage and frequency can be controlled by this component. The effect of frequency will be discussed in chapter 2.4.

In order to minimize stresses on components, the system needs capacitive compensation to ensure that the sending coil operates in resonance. The compensation is located between the inverter and the sending coil, and some basic compensation solutions were introduced in chapter 2.2. The final component on the sending side is the primary coil that is linked magnetically to the secondary coil on the pickup side. Currents in the sending coil induce a magnetic field, which in turn induces a current in the pickup coil. This is the main characteristic of an IPT-system, which makes it possible to transfer through non-conductive materials.

The coil on the pickup side also needs to be compensated to maximize the power transfer capability. The pickup compensation ensures that the secondary coil is also run in resonance during operation. The current induced in the pickup coil needs to be rectified because of the high operating frequency needed for the inductive power transfer. This is why another rectifier is needed to make the current and voltage as smooth as possible before it is fed into the load. This rectifier is usually just a full wave diode rectifier to be more cost efficient. The final step before the load is either an inverter for AC loads or DC/DC converter for DC loads as a final refinery for the output voltage and/or current, but in some cases no converter is needed after the rectifier, as the voltage and current can be controlled to some degree by the sending side inverter. In Figure 2.8 the load is a battery which is charged by the IPT-system. The load depends on the actual application, but IPT-systems are often used to charge batteries, which is the case for wlwctrica vehicled, electrical ferries and most of the commercial WPT applications.

Charging a battery is fundamentally different from having a normal resistive load, because the equivalent load changes according to the amount of energy stored in the battery, defined as "*state of charge*". Additionally, the charging process has two different modes that is illustrated by Figure 2.9. When charging a flat battery, the current is kept constant while the voltage increases linearly. This is called "*constant current-mode"* and is the main mode when charging a battery application. The second mode is the last phase when the linearly increasing voltage has reached the set voltage limit as the battery is near fully charged. The voltage is now kept constant at the limit value V_{max}, while the current decreases exponentially as the battery gets closer to fully charged.

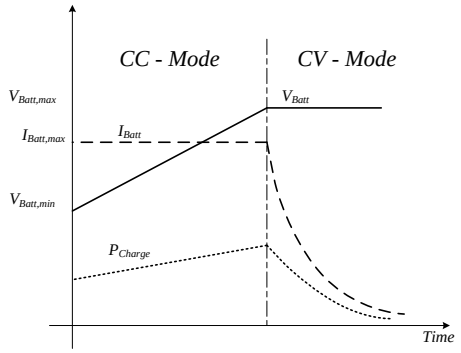

Figure 2.9 shows the charging profile of a battery as a function of time[11].

In short an IPT-system needs to be run in resonance, or at least close to resonance at a certain operation frequency. However, the operating frequency may be changed within a given bandwidth to meet desired control objectives. The control of the outputs mostly relies on the sending side inverter, which governs both frequency and voltage magnitude. But also DC-DC converters can be used either on sending side or receiving side to give more control possibilities.

2.4 The effect of system frequency

The system frequency governs the design and the magnitude of different losses as it is increased. But the operation frequency may be optimized if we look at the IPT-system as a whole and analyse the trade-offs. From eq. (2.4) and (2.5) it is shown that as frequency increases, the efficiency of the coupled coils increase, but an increase in frequency affects much more than just the power transfer between the coils. Especially the switching losses in the power electronics increase as the frequency is increased. An increase in frequency also reduces the dimensions of the coils, which saves material. The seemingly limiting factor is how the switching losses increase linearly as the operation frequency is increased. An analysis of the combined losses of every component of the IPT-system is needed to find the ideal frequency. Research on resonating converters that minimize the switching losses by doing zero voltage switching or zero current switching may help increase the optimum frequency limit. Another thing to consider is the need of the application, and the IPT-systems efficiency is very important with high power applications. Marine and offshore applications typically need power transfers of kW or MW, which are enormous amounts of power.

3 Derivation of the models

In order to determine the design of the control system, the IPT-system has to be represented by mathematical models. A model based on coupled mode theory has been chosen for this thesis, where the envelope of the coil currents and capacitor voltages on both primary and secondary sides are described. This chapter introduces three models:

1. The dynamic model based on the electric circuit of the IPT-system and its dynamic equations.
2. The second model is a nonlinear, averaged time invariant model which describes the envelope of the dynamic model. This is the main model used in this thesis.
3. The final model is a model in Simulink consisting of actual electric components as a control for the purely mathematical models.

The electric circuit that these models are based on is shown in Figure 3.1. The IPT-system is S-S compensated and includes a full bridge inverter on the sending side, and a full wave rectifier on the receiving side. The rectifier and inverter can be represented by square wave voltage sources as shown in Figure 3.2.

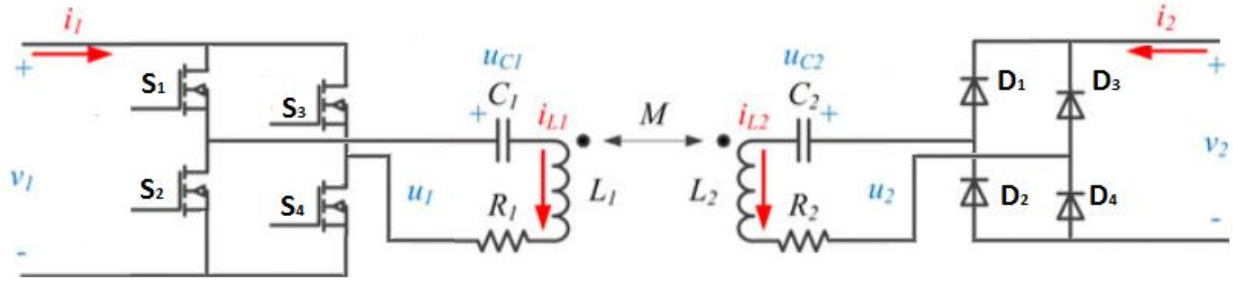

Figure 3.1 shows an S-S compensated IPT-system including the inverter and rectifier[10].

The voltage across the capacitors u_{c1} and u_{c2} and the current running through the coils i_{L1} and i_{L2} are important state variables for the dynamic model. The subscript indicates what side of the IPT-system the parameter is taken from. Where 1 is primary side and 2 is secondary side.

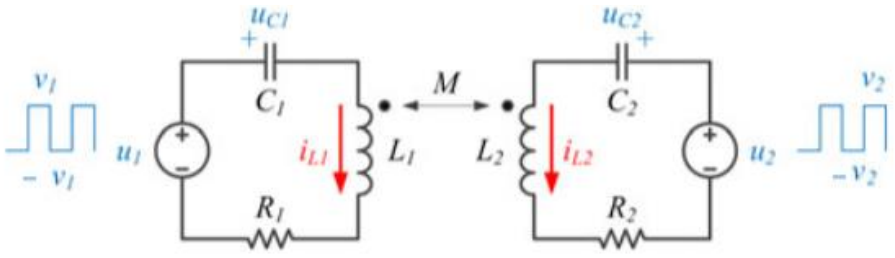

Figure 3.2 shows the simplified circuit of an S-S compensated IPT-system, where the inverter and rectifier are modelled as voltage sources [10].

Figure 3.2 can be expressed mathematically by doing a simple circuit analysis of the IPT-system. The equations in eq. (3.1) make the foundation of the models that are considered in this thesis.

$$\begin{cases} L_1 \frac{di_{L1}}{dt} + M \frac{di_{L2}}{dt} + u_{c1} + R_1 i_{L1} = u_1 \\ C_1 \frac{du_{C1}}{dt} = i_{L1} \\ L_2 \frac{di_{L2}}{dt} + M \frac{di_{L1}}{dt} + u_{c2} + R_2 i_{L2} = u_2 \\ C_2 \frac{du_{C2}}{dt} = i_{L2} \end{cases} \tag{3.1}$$

The parameters that the models are based on are shown in Table 3.1. The parameters are in general set to match a real IPT-system like the prototype at the SINTEF lab in Trondheim. The primary and secondary inductances are taken from this prototype when the air gap is 50mm and no further misalignment, but the inductances need to be adjusted because the frequency used here is different. The resistances on the other hand are primarily set to facilitate the modelling and calculations. The rest of the needed parameters are easily calculated when the inductances, the coupling coefficient and the system frequency are set.

Table 3.1 shows the default parameters for the models (if nothing else is mentioned these values are used)[15].

Parameter		Formula	Value	Comment
System frequency	**(f)**	Set	5 kHz	
Coupling coefficient	**(k)**	Set	0.20	From measurements
Primary inductance	**(L_1)**	Set	35.1 µH*K_f	From measurements
Secondary inductance	**(L_2)**	Set	22.9 µH*K_f	From measurements
Primary resistance	**(R_1)**	Set	1.5 Ω	
Secondary resistance	**(R_2)**	Set	1.5 Ω	
Mutual inductance	**(M)**	$k \cdot \sqrt{L_1 \cdot L_2}$	5.67 µH	
Angular frequency	**(ω_s)**	$2\pi \cdot f$	31415.93 rad/s	
Primary capacitor	**(C_1)**	$\frac{1}{\sqrt{\omega_s{}^2 \cdot L_1}}$	72.0 nF	
Secondary capacitor	**(C_2)**	$\frac{1}{\sqrt{\omega_s{}^2 \cdot L_2}}$	110.61 nF	
Equivalent inductance	**($L_{\sigma 1}$)**	$L_1 - \frac{M^2}{L_2}$	33.7 µH	From eq. (3.2)
Equivalent inductance	**($L_{\sigma 2}$)**	$L_2 - \frac{M^2}{L_1}$	22.0 µH	From eq. (3.2)
Primary resonant angular frequency	**(ω_1)**	$\frac{1}{\sqrt{L_1 \cdot C_1}}$	31415.93 rad/s	
Secondary resonant angular frequency	**(ω_2)**	$\frac{1}{\sqrt{L_2 \cdot C_2}}$	31415.93 rad/s	

In table 3.1the default parameters are shown. A change in the system frequency from assumed 100 kHz in the specialization project to a more realistic frequency of 5 kHz is used to have manageable switching losses. This needs to be compensated for when using the measured self-inductances, which is where the factor Kf is used:

$$Kf = \frac{System\ frequency\ of\ prototype}{System\ frequency\ of\ high\ power\ IPT\ system} = \frac{100000}{5000} = 20$$

The parameters given in Table 3.1 are treated as default settings in this thesis, but later, the parameters like the coupling coefficient and inductances will be changed to simulate coil misalignment.

3.1 Dynamic model

One way to model the dynamics of an IPT-system is to rearrange the circuit equations shown in eq. (3.1), where the parameters i_{L1}, i_{L2}, u_{C1}, u_{C2} are considered to be state variables and u_1 and u_2 are considered as control variables.

$$\begin{cases} L_{\sigma 1}\frac{di_{L1}}{dt} = -R_1 \cdot i_{L1} + \frac{MR_2}{L_2} \cdot i_{L2} - u_{C1} + \frac{M}{L_2} \cdot u_{C2} + u_1 - \frac{M}{L_2} \cdot u_2 \\ L_{\sigma 2}\frac{di_{L2}}{dt} = \frac{MR_1}{L_1} \cdot i_{L1} - R_2 . i_{L2} + \frac{M}{L_1} \cdot u_{C1} - u_{C2} - \frac{M}{L_1} \cdot u_1 + u_2 \\ C_1\frac{du_{C1}}{dt} = i_{L1} \\ C_2\frac{du_{C2}}{dt} = i_{L2} \end{cases} \tag{3.3}$$

Where:

$$L_{\sigma 1} = L_1 - \frac{M^2}{L_2}; \qquad L_{\sigma 2} = L_2 - \frac{M^2}{L_1}$$

By using the rearranged equations in eq. (3.3), a simulation of the transient behavior of the system can be simulated in a Simulink environment. The block named Differential Equation Editor (DEE) has been a vital part to solve and provide the desired outputs from the mathematical models.

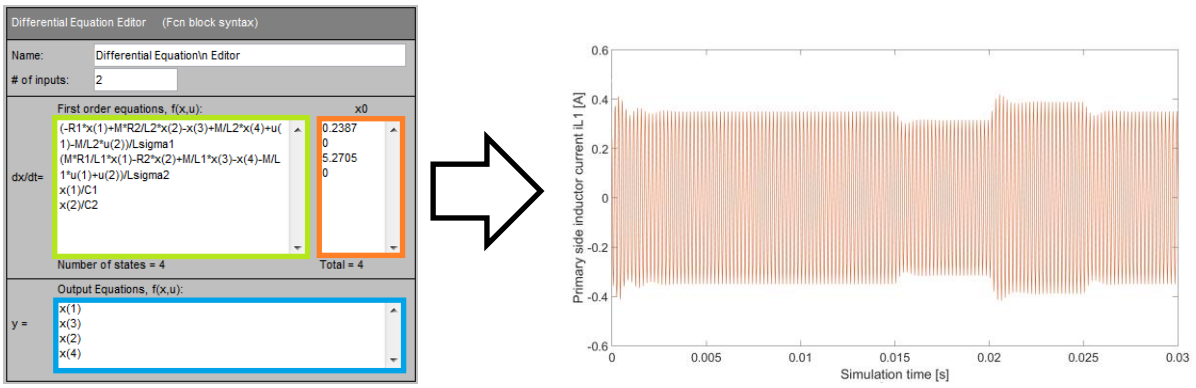

Figure 3.3 shows the DEE block used to simulate the dynamic model, and the output shown graphically for inductor current i_{L1}.

The DEE-block allows sets of first order differential equations to be solved. In Figure 3.3, the equations are inserted in the field marked green, as functions of the state variable and control variables. In the field marked in a blue box the desired outputs are selected. In the orange box the initial conditions are set, which determines the shape of the initial transient.

In the output of the inductor current L_1 shown in Figure 3.3, four transients are present: The initial transient and the three transients that are made by changing the input voltages u_1 and u_2 using step functions in Simulink. U_1 is the input voltage and U_2 is the output voltage, and an increase in the input of the physical system leads to an increase in the output voltage. This is why it is modelled with step changes in both of the inputs. These changes in the inputs are meant to simulate changes in operation conditions which the system may experience during operation. The average model has been simulated in the same simulation and has been given the exact same parameters and input signals.

3.2 Average model

An average model is derived in order to reduce the order and complexity while still having enough information to design the control system for the WPT-system. This model has been based on the findings of Hongchang et al.[10], where coupled mode theory (CMT) is used to model the coupled coils. CMT is a vast field that is well described in Haus and Huang (1991)[19], and it can be applied to passive structures, such as coupled waveguides and coupled resonators. In this thesis only the coupled resonators are relevant for the modelling of the IPT-system, because the coils combined with series compensation can be regarded as a resonating tank. Hongchang et al. have used “coupled energy orthogonal modes of positive energy”[19] and describes the inductor currents and capacitor voltages as functions of the amplitude a_n and the phase of the mode θ_n as shown in eq. (3.4).

$$\begin{cases} i_{Ln} = \sqrt{\frac{2}{L_n}} \cdot a_n \cos(\omega_s t + \theta_n) \\ u_{cn} = \sqrt{\frac{2}{C_n}} \cdot a_n \sin(\omega_s t + \theta_n) \end{cases} \tag{3.4}$$

The first step to deriving the average model is to substitute eq. (3.4-3.6) into eq. (3.1). The results are in the needed format for the DEE block in Simulink. The intermediate results before the averaging of the model are shown in Appendix A. They are compared to the results of Hongchang et al. and sorted like this: to the left are the results straight from Maple Soft by solving the equation sets, while the results as sorted in the paper by Hongchang et al. are on the right.

Note that this thesis differs when deriving the average model based on coupled mode theory compared to Hongchang et al. mainly because of two reasons: Here the converters are full wave instead of half wave, and the dead time of the converter switches are neglected.

$$\begin{cases} \frac{di_{L1}}{dt} = \sqrt{\frac{2}{L_n}} \frac{da_n}{dt} \cos(\omega_s t + \theta_n) - a_n \left(\omega_s + \frac{d\theta_n}{dt}\right) \sin(\omega_s t + \theta_n) \\ \frac{du_{c1}}{dt} = \sqrt{\frac{2}{L_n}} \frac{da_n}{dt} \sin(\omega_s t + \theta_n) - a_n \left(\omega_s + \frac{d\theta_n}{dt}\right) \cos(\omega_s t + \theta_n) \end{cases} \tag{3.5}$$

$$\begin{cases} u_1 = sgn[\cos(\omega_s t)] \cdot v_1 \\ u_2 = -sgn[\cos(\omega_s t + \theta_2)] \cdot v_2 \end{cases} \tag{3.6}$$

In order to simplify the model, a time invariant model is made by neglecting the high frequency terms by averaging the model over one period $\boldsymbol{\omega}_s$. The equations in Figure 3.4 will be the foundation for further investigation of the IPT-system. In the specialization project prior to this thesis the derivation of the average model is better described, but the simulation and verification of the model has been updated in this master thesis. The simulations in which the models are compared and thus verified will be covered in chapter 3.3.

$$\frac{d}{dt} a_1\ averaged = -\frac{L_2 \cdot R_1 \cdot a_1}{2 \cdot \left(L_1 \cdot L_2 - M^2\right)} - \frac{M \cdot \sqrt{L_1} \cdot a_2 \cdot \sin\left(\theta_1 - \theta_2\right)}{2 \cdot \sqrt{C_2} \cdot \left(L_1 \cdot L_2 - M^2\right)} + \frac{M \cdot R_2 \cdot \sqrt{L_1} \cdot a_2 \cdot \cos\left(\theta_1 - \theta_2\right)}{2 \cdot \sqrt{L_2} \cdot \left(L_1 \cdot L_2 - M^2\right)} + \frac{\sqrt{2} \cdot L_2 \cdot \sqrt{L_1} \cdot v_1 \cdot \cos\left(\theta_1\right)}{\pi \cdot \left(L_1 \cdot L_2 - M^2\right)} + \frac{\sqrt{2} \cdot M \cdot \sqrt{L_1} \cdot v_2 \cdot \cos\left(\theta_1 - \theta_2\right)}{\pi \cdot \left(L_1 \cdot L_2 - M^2\right)}$$

$$\frac{d}{dt} \theta_1\ averaged = -\omega_s + \frac{\omega_1}{2} + \frac{L_2 \cdot \sqrt{L_1}}{2 \cdot \sqrt{C_1} \cdot \left(L_1 \cdot L_2 - M^2\right)} - \frac{M \cdot \sqrt{L_1} \cdot a_2 \cdot \cos\left(\theta_1 - \theta_2\right)}{2 \cdot \sqrt{C_2} \cdot a_1 \left(L_1 \cdot L_2 - M^2\right)} - \frac{M \cdot R_2 \cdot \sqrt{L_1} \cdot a_2 \cdot \sin\left(\theta_1 - \theta_2\right)}{2 \cdot \sqrt{L_2} \cdot a_1 \cdot \left(L_1 \cdot L_2 - M^2\right)} - \frac{\sqrt{2} \cdot L_2 \cdot \sqrt{L_1} \cdot v_1 \cdot \sin\left(\theta_1\right)}{a_1 \cdot \pi \cdot \left(L_1 \cdot L_2 - M^2\right)} - \frac{\sqrt{2} \cdot M \cdot \sqrt{L_1} \cdot v_2 \cdot \sin\left(\theta_1 - \theta_2\right)}{a_1 \cdot \pi \cdot \left(L_1 \cdot L_2 - M^2\right)}$$

$$\frac{d}{dt} a_2\ averaged = -\frac{L_1 \cdot R_2 \cdot a_2}{2 \cdot \left(L_1 \cdot L_2 - M^2\right)} + \frac{M \cdot \sqrt{L_2} \cdot a_1 \cdot \sin\left(\theta_1 - \theta_2\right)}{2 \cdot \sqrt{C_1} \cdot \left(L_1 \cdot L_2 - M^2\right)} + \frac{M \cdot R_1 \cdot \sqrt{L_2} \cdot a_1 \cdot \cos\left(\theta_1 - \theta_2\right)}{2 \cdot \sqrt{L_1} \cdot \left(L_1 \cdot L_2 - M^2\right)} - \frac{\sqrt{2} \cdot L_1 \cdot \sqrt{L_2} \cdot v_2 \cdot \cos(0)}{\pi \cdot \left(L_1 \cdot L_2 - M^2\right)} - \frac{\sqrt{2} \cdot M \cdot \sqrt{L_2} \cdot v_1 \cdot \cos\left(\theta_2\right)}{\pi \cdot \left(L_1 \cdot L_2 - M^2\right)}$$

$$\frac{d}{dt} \theta_2\ averaged = -\omega_s + \frac{\omega_2}{2} + \frac{L_1 \cdot \sqrt{L_2}}{2 \cdot \sqrt{C_2} \cdot \left(L_1 \cdot L_2 - M^2\right)} - \frac{M \cdot \sqrt{L_2} \cdot a_1 \cdot \cos\left(\theta_1 - \theta_2\right)}{2 \cdot \sqrt{C_1} \cdot a_2 \left(L_1 \cdot L_2 - M^2\right)} + \frac{M \cdot R_1 \cdot \sqrt{L_2} \cdot a_1 \cdot \sin\left(\theta_1 - \theta_2\right)}{2 \cdot \sqrt{L_1} \cdot a_2 \cdot \left(L_1 \cdot L_2 - M^2\right)} + \frac{\sqrt{2} \cdot M \cdot \sqrt{L_2} \cdot v_1 \cdot \sin\left(\theta_2\right)}{a_2 \cdot \pi \cdot \left(L_1 \cdot L_2 - M^2\right)}$$

Figure 3.4 shows the equations of the averaged model in the desired format[15].

The averaged model is also simulated in Simulink by the use of the DEE block. In order to have control over the four equation sets shown in Figure 3.4, a MatLab script is needed. This script contains the parameters used for both models. It also contains sections that facilitate the insertion of the equations into the DEE block. This main script which has the default parameters and settings is shown in Appendix C

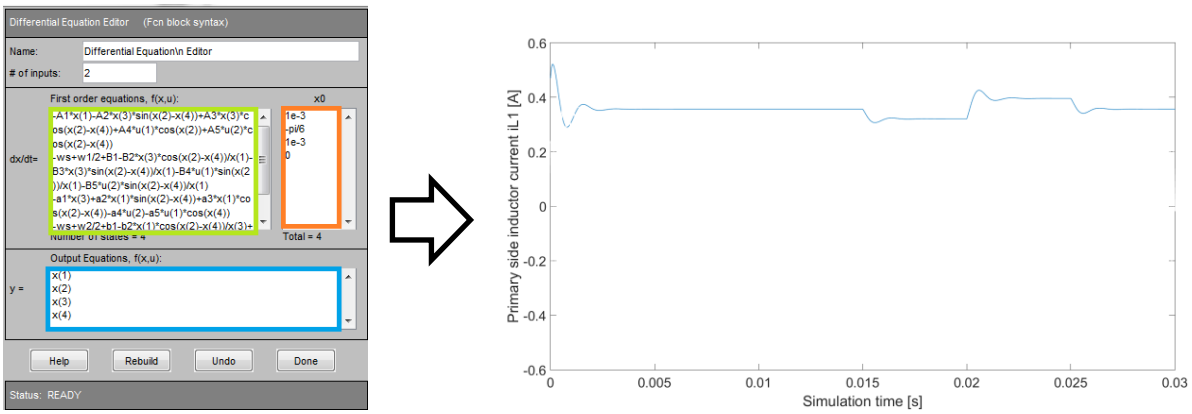

Figure 3.5 shows the DEE block defining the averaged model, including the resulting output of inductor current i_{L1}.

The initial conditions shown in Figure 3.5 in the orange box are set to give a similar start-up transient as the dynamic model, but it is difficult to make a good general configuration of the initial conditions that fit for variations in the simulation parameters. This is why the start-up transient is not considered in detail when making a controller. The default initial conditions will be used unless they lead to instability in the simulations. In the blue window in Figure 3.5 the number of outputs from the block is chosen.

3.3 Simulation for validation of the averaged dynamic model

The first step in verifying the averaged model is to make a Simulink model that has the same settings and parameters, and check if the outputs match the dynamic model. Both of the models have several step-up and step-down blocks multiplied with their inputs to check if the dynamic behavior of the models coincides. Both models are present in Figure 3.6, where the upper DEE block describes the dynamic model and the lower DEE-block describes the averaged model. The dynamic model has two square wave inputs that are phase shifted by 90 degrees, and includes step functions which are included in both the subsystems u(1) and u(2). The phase shift is because of the properties of the mutually coupled inductors.

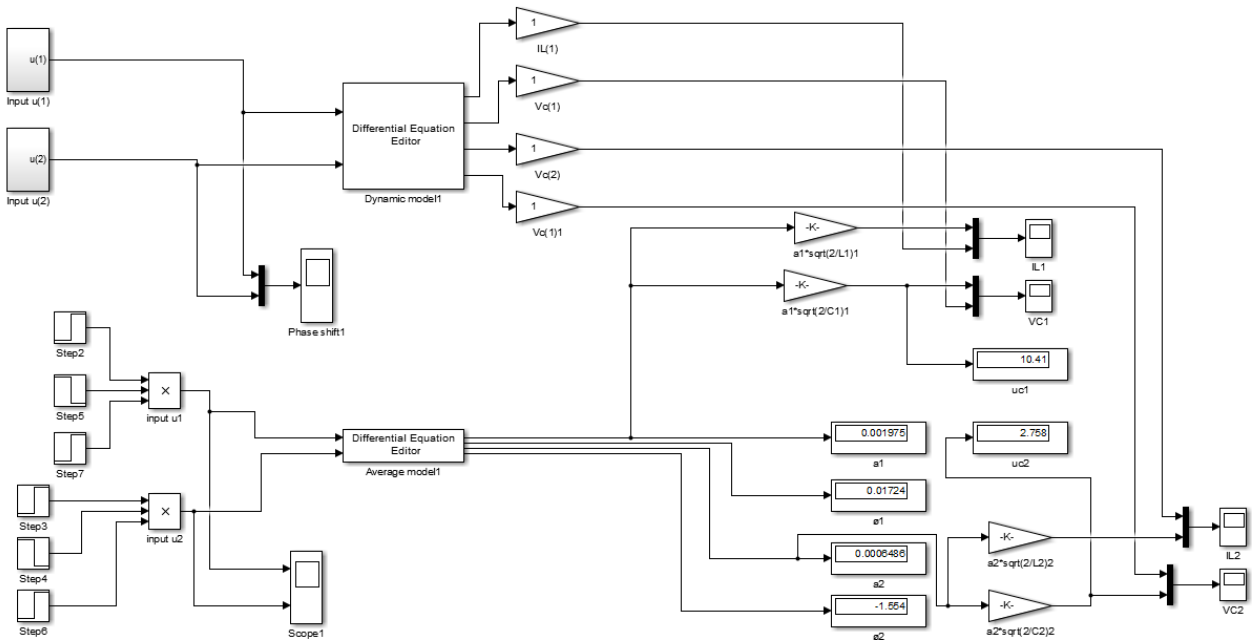

Figure 3.6 shows the simulation that compares the two mathematical models.

The relationship between the outputs of the two models is given by eq. (3.4) and the gain blocks in the model make sure the amplitude of the inductor currents and capacitor voltages are obtained. To keep the simulation manageable, only the amplitudes a_1 and a_2 are considered in this model, because including the phase θ_1 and phase θ_2 would make the model too complicated for the scope of this thesis.

The Simulink model shown in Figure 3.7 shows the resulting inductor current on the primary side when the default settings from chapters 3.1 and 3.2 were used. It is verified that the averaged model works as expected and creates an envelope that covers the positive amplitude of the dynamic model. Except for the initial transient, the model reacts quite correctly to sudden changes in the system amplitude. In Figure 3.7 the dynamic model is oscillating plot in red, while

the averaged model is the blue curve that follows the amplitude of the dynamic model in red. Similar results are obtained from the other outputs too.

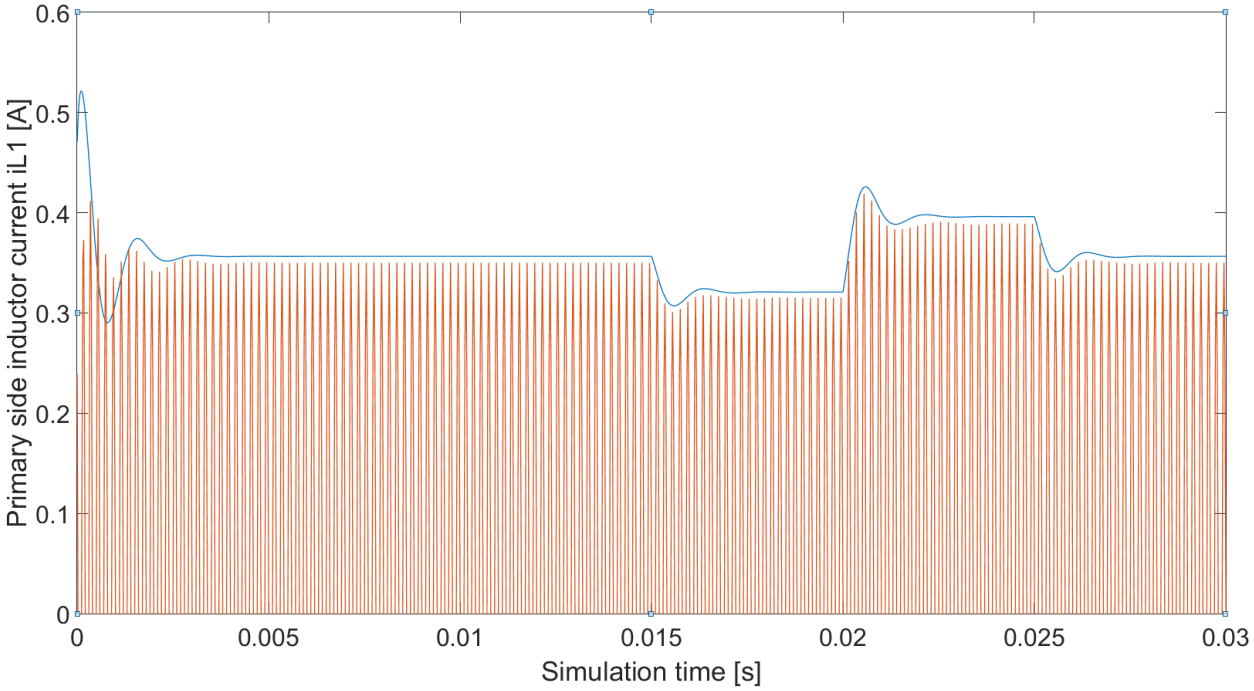

Figure 3.7 shows the resulting primary inductor current i_{L1} from both the DEE blocks.

By verifying that the averaged model is a good approximation, it is appropriate to linearize the averaged model at stable operating points where the transient has settled. The linearized model is then used to extract a transfer function of the input voltage to the output current.

4 Control theory

This chapter will explain some basic control theory terms, and cover much of the methodology that has been used to design a controller for the IPT-system. This chapter does not contain specific results from the MatLab scripts, but will explain how and why the controller is needed and designed, and finally show the different types of controllers.

When designing a control system for an electrical application, the basic equations derived from ohm's law and Kirchhoff's laws are the foundation of the model used to analyze the system. But real systems are often too complicated to create an exact model of, which is why engineers have to spend a lot of time applying correct approximations. The approximations have to both simplify the mathematical model of the system and preserve the system behaviour as close to the real system as possible.

The basic equations derived from ohm's and Kirchhoff's laws provide a differential equation that can describe the relationship between an input r(t) "reference point" and the output y(t) "controllable variable". In eq. (4.1) the general form of a linear, time-invariant differential equation is shown[20].

$$a_n \frac{d^n c(t)}{d(t)^n} + a_{n-1} \frac{d^{n-1} c(t)}{d(t)^{n-1}} + \ldots\ldots + a_1 \frac{dc(t)}{dt} + a_0 y(t) = b_m \frac{d^m r(t)}{d(t)^m} + b_{m-1} \frac{d^{m-1} r(t)}{d(t)^{m-1}} + \ldots\ldots + b_1 \frac{dr(t)}{dt} + b_0 r(t) \quad (4.1)$$

The basic equations describing the S-S-compensated IPT-system are shown in eq. (4.2), and because there are four energy storages present in the IPT-system, four equations are needed. Thus this is a fourth order system.

$$\begin{cases} L_1 \frac{di_{L1}}{dt} + M \frac{di_{L2}}{dt} + u_{c1} + R_1 i_{L1} = u_1 \\ C_1 \frac{du_{C1}}{dt} = i_{L1} \\ L_2 \frac{di_{L2}}{dt} + M \frac{di_{L1}}{dt} + u_{c2} + R_2 i_{L2} = u_2 \\ C_2 \frac{du_{C2}}{dt} = i_{L2} \end{cases} \quad (4.2)$$

Where u_1 and u_2 are signum functions with v_1 and v_2 as the magnitudes of the inputs, this is shown in eq. (3.5). The basic equations are further developed to give the desired mathematical model of the IPT-system as shown in chapter 3.2.

The goal of the mathematical model is to derive the relationship between the input and output. There are two popular methods to do this: Transfer functions in the frequency domain, and state equations in time domain. This thesis will focus on modelling in frequency domain, and the

sending side voltage (v_1) is chosen as the input, while the receiving side current (i_2) is chosen as output.

4.1 Modelling in frequency domain

When representing a physical system in a mathematical model, the input and output should be in separate entities. Another attribute that is desired is the ability to model several subsystems more easily. From the differential equation shown in eq. (4.1), the input and output are not easily separated. This is where the Laplace transform makes handling systems based on differential equations easier to handle mathematically by transforming the system from time domain to frequency domain.

$$\mathcal{L}[f(t)] = F(s) = \int_{0-}^{\infty} f(t)e^{-st}\,dt \tag{4.2}$$

Where s is a complex variable on the form: ($s = \sigma + j\omega$). Thus, there is a Laplace transform of the function f(t) if the integral shown in eq. (4.2) converges[20]. Notice that the lower limit of the integral is "0-", which implies that even if the initial conditions at t=0 is discontinuous, the integration can start prior to the discontinuity. As this property of the Laplace transform ensures that even though most differential equations are discontinuous at the initial conditions, they can be transformed to frequency domain as a Laplace function by knowing the initial condition before the discontinuity.

By the use of Laplace transformation on the equations representing a physical system, we can make a transfer function for this system. A transfer function allows the separation of the input, output and system into three separate parts. Additionally, transfer functions allow simple algebraic mathematics to be sufficient when combining subsystems.

Our IPT-system has four energy storages, which implies that it can be modelled as a fourth order system. To explain the transfer function of a 4th-order system a 4th-order, linear, time-invariant differential equation is enough:

$$a_4\frac{d^4y(t)}{d(t)^4} + a_3\frac{d^3y(t)}{d(t)^3} + a_2\frac{d^2y(t)}{d(t)^2} + a_1\frac{dy(t)}{dt} + a_0y(t) = b_4\frac{d^4r(t)}{d(t)^4} + b_3\frac{d^3r(t)}{d(t)^3} + b_2\frac{d^2r(t)}{d(t)^2} + b_1\frac{dr(t)}{dt} + b_0r(t) \tag{4.3}$$

Where $y(t)$ and $r(t)$ are output and input respectively, and the a's, b's and the form of the differential equation depends on the parameters of the IPT-system. By taking the Laplace transform on both sides we get:

$$(a_4s^4 + a_3s^3 + a_2s^2 + a_1s^1 + a_0)\,Y(s) = (b_4s^4 + b_3s^3 + b_2s^2 + b_1s^1 + b_0)\,R(s) \tag{4.4}$$

Now the ratio between the output and input is easily found and the three entities are separated:

$$\frac{Y(s)}{R(s)} = G(s) = \frac{(b_4s^4+b_3s^3+b_2s^2+b_1s^1+b_0)}{(a_4s^4+a_3s^3+a_2s^2+a_1s^1+a_0)} \tag{4.5}$$

The ratio G(s) is called the transfer function of the system, and it is evaluated with zero initial conditions. Systems in frequency domain are often presented as a block diagram where blocks between the output and input represents the transfer functions representing the different subsystems. Block diagrams is a mathematical modelling method that is a very important tool to show complex systems more intuitively. This shows how a transfer function is a function connecting the input to the output. Although in this thesis the fourth order IPT-system will first be described by a state space model in time-domain before extracting the transfer function between the sending side voltage and the receiving side current.

4.2 Modelling in time domain

The modelling in frequency domain in chapter 4.1 is often called the classic method, which has several advantages when it comes to modelling simple systems. With the classic method it is quick and intuitive to test the step response of a system and check the stability. Even though it is an efficient and intuitive method, it has more limitations and drawbacks compared to modelling in time domain. Transfer functions only exist if the system is a linear, time-invariant system or can be approximated as such. More complex systems with several inputs and outputs cannot be modelled in frequency domain.

The method using time domain is referred to as state space- or modern approach, and is applicable on both nonlinear systems and linearized systems. Even systems with several inputs and outputs can be modelled using state space approach, but this method is not as intuitive. More calculation and more understanding of the system and the differential equations are needed to grasp the physical understanding of changes in parameters when using state space.

To explain the derivation of a state space model, some parameters needs to be defined: State variables, system variables and state equations. State variables are variables that are linearly independent, which means that you cannot express a state variable algebraically using other state variables. The system variables are variables that can be evaluated algebraically from the state variables and the input(s). The state equations are simultaneous, first order differential equations which define each state variable, and normally the number of state variables and state equations are equal to the order of the system. Here is a list of how to derive the state space model[20]:

1. Select the proper state variables.
2. Check the order of the system and write that many simultaneous differential equations in terms of the state variables.
3. If the initial conditions t_0 of the state variables and the inputs $t \geq t_0$ are known, the differential equations can be solved for the state variables for $t \geq t_0$.
4. Then by solving the state variables and inputs for $t \geq t_0$ algebraically, the other system variables are found. This algebraic equation is called the output equation.

5. The state equations and the output equation combined with the input and state variables give us the state space representation of the system in the form:

$$\dot{x} = Ax(t) + Bu(t)$$
$$\dot{y} = Cx(t) + Du(t) \qquad (4.6)$$

Where: $\dot{x}$ = time derivative of the state vector, $\dot{y}$ = time derivative of the output(s),
$x(t)$ = the state vector containing each of the state variables
$u(t)$ = the input or control vector
A = system matrix (jacobian matrix), B = input matrix,
C = output matrix, D = feed forward matrix

4.3 Linearization of the nonlinear averaged model

The nonlinear averaged time-invariant model shown in chapter 3.2 is a fourth order system defined by the equations shown in Figure 3.4. The state variables are defined as sending side mode amplitude a_1 and phase angle θ_1 and receiving side mode amplitude a_2 and phase angle θ_2. The IPT-system can be represented as one compact block as shown in Figure 4.1, where x is the state vector, $v_1$and v_2 are the inputs and f is the state equations from Figure 3.4 expressed as a vector.

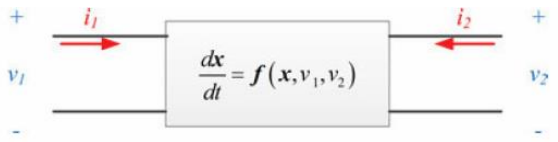

Figure 4.1 shows the compact format of the IPT-system.

Where:

$$x = \begin{pmatrix} a_1 \\ \theta_1 \\ a_2 \\ \theta_2 \end{pmatrix}, \quad f = \begin{pmatrix} f_1 \\ f_2 \\ f_3 \\ f_4 \end{pmatrix} \text{ and } \frac{dx}{dt} = \begin{pmatrix} \frac{da_1}{dt} \\ \frac{d\theta_1}{dt} \\ \frac{da_2}{dt} \\ \frac{d\theta_2}{dt} \end{pmatrix}$$

The currents i1 and i2 from Figure 4.1 are the average port currents during a switching period. They are chosen to represent the model's outputs and can be expressed using the state variables. From Hongchang et al. the relationship between the state variables and the output currents is found to be [10]:

$$\begin{cases} i_1 = g_1(x) = \frac{1}{\pi}\sqrt{\frac{2}{L_1}}a_1\cos(\theta_1) \\ i_2 = g_2(x) = -\frac{1}{\pi}\sqrt{\frac{2}{2}}a_2 \end{cases} \quad \text{and} \quad g(x) = \begin{pmatrix} g_1(x) \\ g_2(x) \end{pmatrix} \tag{4.7}$$

Modelling in time domain is used in this thesis as a stepping stone to achieve the desired transfer function, which is to be used for further studies. The transfer function from input voltage v_1 to output i_2 (see Figure 3.1) is extracted from the state space model after the linearization of the nonlinear averaged model is performed.

4.3.1 Why a linearized model is desired

In control theory we differentiate between linear systems and nonlinear systems. The practical difference between the two is the fact that it is relatively easy to handle linear systems compared to nonlinear systems. A linear system must possess two properties: Superposition and homogeneity. Superposition means that the output response of a system to the inputs is the sum of the responses from each of the individual inputs[20]. If input $r_1(t)$ yields an output $y_1(t)$ and $r_2(t)$ yields response $y_2(t)$, then the sum of the inputs give this result: $r_1(t) + r2(t) = c_1(t)+c_2(t)$. The property homogeneity describes how the system responds to a multiplication of the input by a scalar. The response of a linear system has to include the same scalar as the scalar multiplied by the input. Shown by symbols: A*r1(t) = A*c1(t). Only if both of these properties are present the system can be regarded as linear.

The definition of a linear system is quite strict, and few practical systems are linear in every part of their field of operation. Effects like saturation, deadzone, friction and other complex phenomena leads to nonlinearities, but we can linearize nonlinear systems around a stable operating point. If any nonlinear components are present in the system, it is necessary to linearize the system to be able to define a transfer function for the system.

4.3.2 Jacobian linearization and Jacobian matrices

When linearizing the nonlinear averaged model, the Jacobian linearization method is used to make a small signal representation of the IPT-system. The compact representation of the IPT-system from Figure 4.1 will be used.

$$\dot{x} = f(x, u) \tag{4.8}$$

Where: x is the state vector and u is the input vector: $\begin{pmatrix} v_1 \\ v_2 \end{pmatrix}$

The first step is to spot the nonlinear component and derive the nonlinear differential equations. The nonlinear differential equation is linearized for small inputs around an equilibrium point. The equilibrium point is where the system is at steady state for a given equilibrium input, such that[21]:

$$f(\bar{x}, \bar{u}) = 0 \tag{4.9}$$

Where: $\bar{u} = equilibrium\ input\ and\ \bar{x} = equilibrium\ point$

At the equilibrium point, we know that at a constant equilibrium input the state of the system will stay fixed at $x(t) = \bar{x}$ for all t. But we are not interested in what happens exactly at steady state, which is why we introduce deviation variables to study small changes of input around the equilibrium point.

$$\delta x(t) = x(t) - \bar{x} \tag{4.10}$$
$$\delta u(t) = u(t) - \bar{u} \tag{4.11}$$

This relabelling of variables defines the equilibrium point as the systems zero. This allows the variables $x(t)$ and the inputs $u(t)$ to be related by the differential equation in eq. (4.1).

By substituting eq. (4.10) and (4.11) into eq. (4.8), we get:

$$\dot{\delta} x(t) = f(\bar{x} + \delta x(t), \bar{u} + \delta u(t)) \tag{4.12}$$

In order to linearize this differential equation, a Taylor expansion of the right hand expression is made, where the higher (higher than first) order terms are neglected.

$$\dot{\delta} x(t) \approx f(\bar{x}, \bar{u}) + \frac{df}{dx}\delta x(t) + \frac{df}{du}\delta u(t) \approx \frac{df}{dx}\delta x(t) + \frac{df}{du}\delta u(t) \tag{4.13}$$

Where $f(\bar{x}, \bar{u}) = 0$

Since the higher order terms are neglected, we can consider this a linear differential equation that approximately govern the deviation of the variables $\delta x(t)$ and $\delta u(t)$, but only if the deviations are small. It is important to remember the connection between the normal parameters and the small signal parameters ($\delta x, \delta u$) that is shown in eq. (4.10) and (4.11)

$$A \coloneqq \frac{df}{dx} \in R^{4\times4} \qquad B \coloneqq \frac{df}{du} \in R^{4\times2} \tag{4.14}$$

The matrices A and B are constant matrices, and we can define the linearized system as:

$$\dot{\delta} x(t) = A\delta x(t) + B\delta u(t) \tag{4.15}$$

This is called the Jacobian Linearization of the nonlinear system, close to the equilibrium point $(\bar{x}, \bar{u})$. This linearization provides a very good approximation to the nonlinear system when the deviations are small. The same procedure is used to derive the matrices which describe the small signal output.

$$\dot{\delta} y(t) = C\delta x(t) + D\delta u(t) \tag{4.16}$$

Where the matrices C and D are given by these expressions for the IPT-system:

$$C \coloneqq \frac{dg}{dx} \in R^{2\times 4} \qquad D \coloneqq \frac{dg}{du} = 0{*}R^{2\times 2} \tag{4.17}$$

Now the linearized state space model for the IPT-system is defined by the four matrices: A, B, C and D. The matrices are changed according to the configuration of the IPT-system and the choice of equilibrium point. As equilibrium point, the final steady state value is used. The Matlab-script shown in Appendix C uses the information from the parameters of the IPT-system, and the equilibrium point is found by running a simulation in Simulink for each configuration of the coupling. By using the linearized matrices, the script derives the matrix of transfer functions G(s):

$$G(s) = \begin{bmatrix} \frac{\hat{\imath}_1}{\hat{v}_1} & \frac{\hat{\imath}_1}{\hat{v}_2} \\ \frac{\hat{\imath}_2}{\hat{v}_1} & \frac{\hat{\imath}_2}{\hat{v}_2} \end{bmatrix} = C \times (s * I - A)^{-1} \times B \tag{4.18}$$

The transfer function marked in yellow in eq. (4.18) is the only transfer function that will be used when designing the controller. This is because the input voltage is set and controlled by the inverter, and the output current to the receiving side is the most important output to control. The actual results from the MatLab scripts and the Simulink model of the changes in the transfer function will be covered in chapter 5.

4.4 Second order approximation

In order to have simple analytical expressions of how a system responds, it is advantageous to model higher order systems by making a second order approximation model of the system. But not every higher order system may be represented accurately by a second order equivalent. Figure 4.2 shows some examples of second order systems and how the configuration of the poles defines the response of the system. The poles must be in the left half-plane in order to have a stable system. Two purely real poles result in an overdamped step response without any oscillations around the final value, while two purely imaginary poles means the system is undamped and oscillates around the final value. Typically poles have both a real part (σ) and one imaginary part ($j\omega$) and they always occur in pairs on the form: $\sigma \pm j\omega$. The complex poles give an underdamped response. This response does not settle at the final value immediately, but have damped oscillations that eventually settle at the final value according to the ratio between the real and imaginary part of the poles.

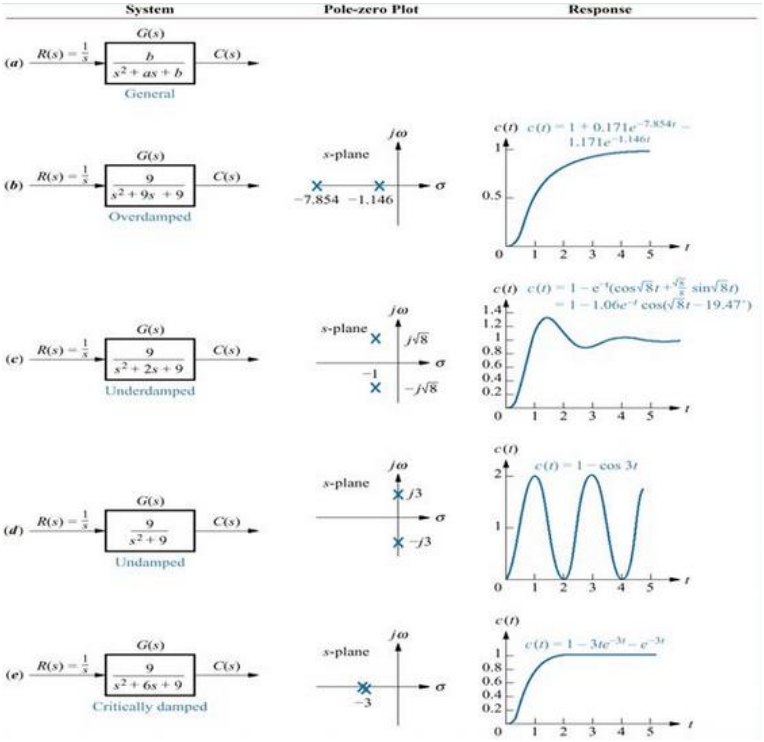

Figure 4.2 shows different configurations of second order systems: transfer functions, poles and step responses[20]

Before the equations for a general second order system is shown, two definitions need to be introduced. First is the frequency of the oscillations of the second order system without damping, which we define as: "*natural frequency*" (ω_n). For electrical systems this refers to the system response if the resistance is neglected and only capacitors and inductors are present. The second definition is called "*damping ratio*" ($\boldsymbol{\xi}$). This parameter is defined as a measure of exponential decay frequency of the envelope to the natural frequency[20]:

$$\xi = \frac{\text{Exponential decay frequency}}{Natural\ frequency\ (rad/s)} = \frac{1}{2\pi}\ \frac{Natural\ period\ (seconds)}{Exponential\ time\ constant} \tag{4.19}$$

As mentioned earlier, the modelling will be in frequency domain using transfer functions. A general second order system can be modelled by this transfer function:

$$G_{2nd}(s) = \frac{b}{s^2+as+b} \tag{4.20}$$

For an undamped system the coefficient a is zero which makes the natural frequency by definition equal to square root of b. Also assuming that the system is underdamped and has a complex pole where the real part, σ, then is equal to $-a/2$. The magnitude of σ is then the exponential decay which is part of the definition of the damping ratio. This means that:$\xi = \frac{|\sigma|}{\omega_n} = \frac{a/2}{\omega_n}$ and $\omega_n = \sqrt{b}$. Thus, the general second order system can be represented using only ξ and ω_n:

$$G_{2nd}(s) = \frac{\omega_n^2}{s^2+2\xi\omega_n s+\omega_n^2} \tag{4.21}$$

The second order approximation is desirable because these systems are well covered in literature, and most of the important system parameters have simple analytical expression. This makes the design of a controller for second order approximations more systematic and efficient, but the approximation must be verified before the design of the controller can begin.When we are approximating the higher order IPT-system to a simple second order system, there are some rules of thumb that is utilized.

4.4.1 Neglecting poles located far from the dominating pole(s)

According to Nise[20], the effect of an additional pole may be neglected if the pole is located at least five times as far away from origin as the dominating poles on the real axis in the s-plane. This is because in time domain the real part of a pole determines the exponential decay. But this is only an approximation which should be verified either by simulation or performing a partial fraction expansion. If the other poles are negligible, the system can be represented by only the dominant poles. For an underdamped system, the dominating poles are always the complex pole pair closest to the origin. For other systems it is the pole closest to origin, except if a pole is in the right half plane of the S-plane, but this means the system is unstable.

4.4.2 The effect of a zero and zero/pole cancellation

Adding a zero to a second order system does not change the nature of the response, but rather change the amplitude and residues of it. In general, the effect of adding a pole can be analyzed in Laplace domain by multiplying a transfer function C(s) by a zero (s+a) that gives the response C(s):

$$(s+a)C(s) = sC(s) + aC(s)$$

Thus, the effect of a zero on the response can be separated into two parts; one derivative part of the original response, and a scaled version of the original response. This means that if a is very large, the Laplace transform of the response can be regarded as equal to $aC(s)$. This means that if a pole is located far from the origin compared to the dominating poles, it can be regarded as a constant with the value a. If the zero is located close to the dominating poles, the derivative term prevails and may increase overshoot and has more effect on the response. Zeroes can only be simplified if they are located far from the dominating poles or if they can be cancelled by a pole in Laplace domain.

Let us consider a third order system with a dominant pole pair and one pole along the real axis with a zero which is close or equal to the third pole:

$$T(s) = \frac{K(s+z_1)}{(s+p_3)(s^2+as+b)}$$

If $z_1 = p_3$ the zero cancels out the pole perfectly and T(s) becomes a second order system. But that rarely happens with real systems that have identical poles and zeroes. This makes it necessary to determine when a zero and a pole are similar enough to cancel each other. This clearly depends on the desired accuracy, and is determined by partial-fraction expansion of the transfer function that allows the contribution from each pole to be compared. Depending on the desired accuracy, the third pole may be cancelled if its contribution is much less than the other poles. Nise propose that around two magnitudes of difference are enough to cancel the zero with the third pole with acceptable accuracy.

By using the rules, our IPT-system may be approximated to a second order system which allows well defined analytical expressions for the control design criteria. First the second order approximation must be verified through simulation.

4.5 System control criteria

When a control engineer evaluates a system, he often measures three general properties of a system: the stability, the transient response and the steady state error of the system. Parameters which characterize each of the general properties need to be calculated and dimensioned to fit the purpose of the system. The three design criteria will be explained and be linked to the design of this IPT-system design.

4.5.1 Stability

Stability is the most important requirement for a control system as both the other properties of a system becomes meaningless for an instable system. In this thesis only linear time-invariant (LTI) systems will be considered, and for these systems there are definitions for: stable, unstable and marginally stable systems. The output y(t) can be divided into two parts for a linear system:

$$y(t) = y_{forced}(t) + y_{natural}(t)$$

The forced response is the actual change in input, but the natural response is an oscillation which depends solely on the system. The most basic definition of stability defines a system stable if a bounded input produce a bounded output, which means that the natural response goes to zero as time approaches infinity. On the other hand, if the natural response does not reduce to zero as time approach infinity, we define the system either unstable or marginally stable. If the response grows towards infinity it is definitely unstable, but if the system is undamped and oscillate with the same magnitude forever, it can be considered marginally stable. Note that an unstable system will destroy itself if no safety measures are included in the design. Both marginally stable and unstable systems are undesirable for our IPT-system. The IPT-system has to be **stable.**

4.5.2 Transient response

The transient response refers to how the system behaves in time domain when changes in the input are done. In Figure 4.3 the input is a step function, which is the type of input function that will be used in this thesis. Here, the transient response can be quantified according to certain parameters. The transfer functions are fourth order, but as a first estimation second order approximations will be made to model the system. For second order systems the transient response is well defined with analytical expressions for the parameters describing the transient behaviour. The parameters are summarized in Figure 4.3 and the equations are shown only for second order systems that are on the form defined in eq. (4.21).

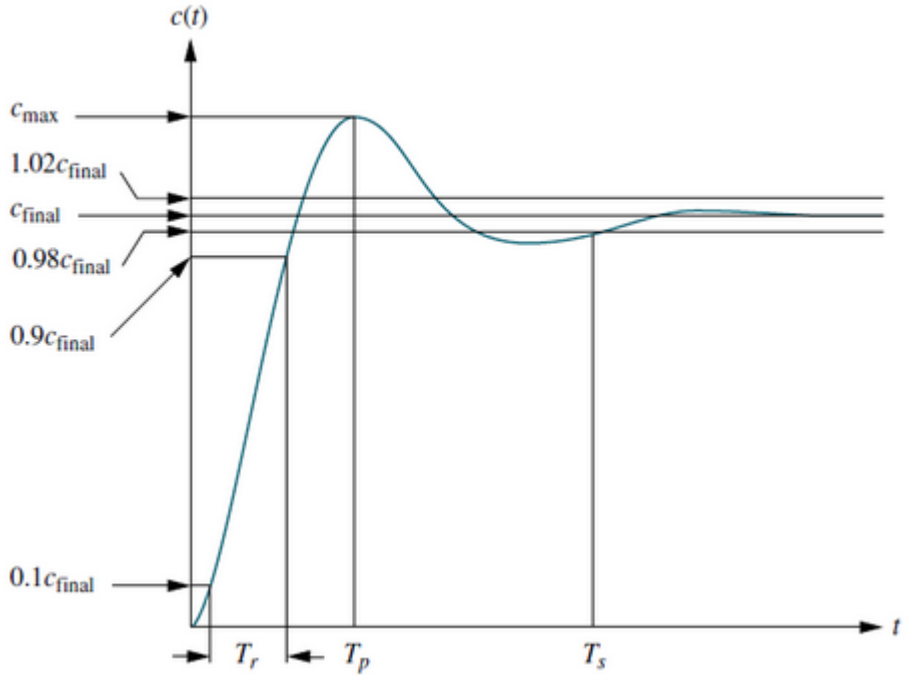

Figure 4.3 shows the step response and define the different parameters of a second order system with a step input[20]

Risetime (Tr):

The time it takes the step signal to go from 10% of final value to 90% of final value is defined as the rise time. There is no accurate analytical relationship between the rise time and the damping ratio ξ. Instead, it is common to set $\omega_n t$ as the normalized time variable and set the value of ξ. Then, the normalized rise time ($\omega_n T_r$) in Figure 4.4 is the graph created by solving the difference between the values of $\omega_n t$ that give 90 and 10 percent of the final value when the damping ratio is set. By using a computer to solve for different values of ξ the graph is made, but this is only valid for underdamped second order systems at ξ=0.1 to 0.9.

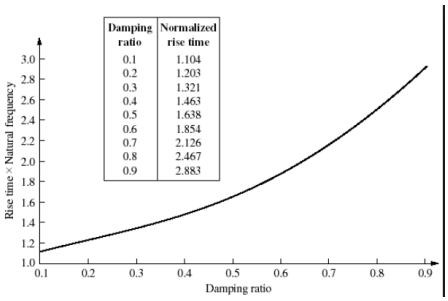

Figure 4.4 shows the normalized rise time for a second order under damped response vs. damping ratio[20]

Peak time:

The time it takes the transient to reach the first peak is defined as the peak time (Tp)

$$T_p = \frac{\pi}{\omega_n\sqrt{1-\xi^2}}$$

Percent overshoot (%OS)

The relative difference in magnitude between the peak and the final value is normalized using the final value as the reference. The normalized peak overshoot is referred to percent overshoot (%OS) typically measured in percent.

$$\%OS = \frac{c_{max} - c_{final}}{c_{final}} = e^{-\left(\frac{\xi\pi}{\sqrt{1-\xi^2}}\right)} \times 100$$

The overshoot is only dependent on the damping ratio $\boldsymbol{\xi}$, which means that the damping ratio easily can be read from the step response of a second order system/ approximation:

$$\xi = \frac{-\ln(\%\,OS/100)}{\sqrt{\pi^2 + ln^2(\%\,OS/100)}}$$

Settling time:

The time it takes the transient amplitude to reach below two percent of the final value is defined as the settling time.

$$T_s = \frac{-\ln(0.02\sqrt{1-\xi^2})}{\xi\omega_n} \approx \frac{4}{\xi\omega_n}$$

The step response mostly tells about the speed of the system and how the transient behaves when the input changes. The damping ratio is an important factor which defines much of how the transient response behaves. For a second order system the damping ratio and natural frequency is easy to determine, and thus the transient response analysis is quite straight forward.

Most of the applications receiving power from an IPT-system tolerate settling times of seconds and overshoot is not a great problem for short durations, but it should be kept under control. For example, a battery ferry is connected for several minutes each time it reach the docks, thus reaching final value after some seconds is acceptable.

4.5.3 Steady state

Another important design objective is the steady state of a system. Ideally, the output should settle exactly at the desired value. But this is not always the case, thus a steady state error is defined as the difference between the given input and the resulting output. Typically, three types of system inputs are used for control systems: Step function for constant position, ramp function for constant velocity and parabola for constant acceleration. The IPT-system uses a step input, so only step input will be covered. In Laplace domain a step input is described as 1/s. The steady state error E(s) is defined as input R(s) minus output Y(s) and can be modelled using a unity feedback block diagram.

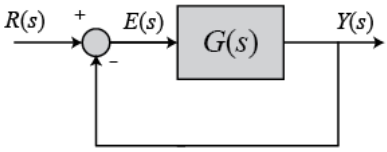

Figure 4.5 shows a general unity feedback system represented as a block diagram

Several steady state errors in control systems come from nonlinear sources like gear backlash and start-up voltage limit of a motor, but nonlinear sources are not considered in this thesis. Apart from nonlinearities, the IPT-system itself and the input type introduce a steady state error.

When calculating the resulting error, the final value theorem is used. By analysing a unity feedback system as time approaches infinity or in Laplace domain when "*s*" approaches zero, the steady state error can be measured for any transfer function which is stable.

$$e(\infty) = \lim_{s\to 0} \frac{sR(s)}{1+G(s)} \tag{4.7}$$

In eq. 4.7 the final value theorem is shown and R(s) is the step input (1/s) that cancels the "s" in the numerator. This means that the error depends on the value of G(s) as "*s*" approaches zero, the greater the value of G(s) is the less the error becomes. This means that a gain introduced in the forward loop results in lower error, but at the same time increases the overshoot of the system. By

introducing integrator (1/s) in the forward loop and still have a step input, the resulting error becomes zero as 1/s*G(s) approaches infinity. The integrator can give an output even if there is no input, but it also makes the settling time and rise time longer, thus slowing down the system. Electrical systems with a gain compensation to reduce steady state error can be achieved by using passive elements. Introducing an integrator to eliminate the error completely requires active components that might need their own voltage source, although recent development of power electronics has reduced the downside of active compensators.

To summarize, the stability of a system is a prerequisite for any control system in order to control the output and set the other two criteria. Trade-offs needs to be made between the improvements of the step response vs. the steady state error. Everything needs to be taken into account when designing a controller. For the IPT-system it is very important that the output going to the application is within its specification voltage and current. Introducing an integrator as a compensator and have zero error would be preferable, as long as it does not slow down the system too much.

4.6 Basic controller designs

As shown in chapter 4.5, there are three general design criteria for a control system. Each of these criteria has to be within certain limits to work as intended, but this rarely is the case for real non ideal systems. The IPT-system is designed to be efficient and to be able to transfer large amounts of power, but this does not necessary give good control design. This is why instead of directly making the changes to the system, additional zeros and poles may be added to the system in cascade or in a feedback loop as compensation[20]. The added zeroes and poles can reduce or even eliminate steady state error, and can improve the step response of the system.

There are three basic forms of compensation: pure gain controller, integral controller, and derivative controller. Compensation by pure gain results in reduced steady state error, but at the same time increase the percent overshoot of the transient response. Integral compensation is used to reduce the steady state error while keeping the transient response close to the original response. The derivative compensation improves the transient response while keeping the steady state error unchanged or even improved. In Table 4.1 the controllers: PI, PD and PID are ideal compensators, where P stands for proportional, I for integral and D for derivative. The ideal compensators may reduce the steady state error to zero and improve the transient response, but there are a few drawbacks. One drawback is that these compensators require active components that mean increased cost for more advanced power electronics. The derivative term in both PD and PID creates noise which grows proportional to the frequency. This causes trouble for the system at higher frequencies and lead to saturation and system failure.

Table 4.1 shows a summary of the different basic controllers; their function, Transfer function and other characteristics[20].

Compensator	Function	Transfer function	Characteristics
Pure gain	Reduce steady state error	K	Increase overshoot
PI	Eliminate steady state error	$K\frac{s+Z_c}{s}$	1. Increase system type 2. Error becomes zero 3. Active circuits required
Lag	Reduce steady state error	$K\frac{s+Z_c}{s+P_c}$	1. Error does not become zero but is improved 2. Active circuits are not required
PD	Improve transient response	$K(s+Z_c)$	1. Active circuits are needed 2. May cause noise and saturation in transient response
Lead	Improve transient response	$K\frac{s+Z_c}{s+P_c}$	1. Pole at -P_c is more negative than zero at -Z_c 2. Active circuits are not required
PID	Improve both steady state error and transient response	$K\frac{(s+Z_{lag})(s+Z_{lead})}{s}$	1. Zero at –Z_{lag} reduce steady state error 2. Zero at –Z_{lead} improves transient response 3. Active circuits required
Lag-lead	Improve both steady state error and transient response	$K\frac{(s+Z_{lag})(s+Z_{lead})}{(s+P_{lag})(s+P_{lead})}$	1. Increase system type 2. Error becomes zero

Another technique is to make compensator from passive elements like resistors, inductors and capacitors. These are not considered ideal compensator, but they are cheaper, and do not require additional power sources. Additionally, the noise and saturation is cancelled when using a non-ideal derivate (lag-compensator). The disadvantages are mainly that the steady state error can only be reduced, not eliminated as an ideal integrator does. Such compensators are called lag- and lead compensator that represents integral compensation and derivative compensation respectively. In Table 4.1 it is clear how the transfer functions are different between the ideal and non-ideal compensation. The design of compensation will be done in frequency domain and only the lag, lead and combinations of them will be considered. This is due to the advantages mentioned and because the modelling in frequency domain facilitates the design of non-ideal compensators.

5 Modelling and analysis of the transfer functions

In chapter 3, the mathematical models of the IPT-system are shown, and in this chapter the nonlinear, averaged time-invariant model will be linearized. From the linearized model, the transfer function between the input voltage "v1" and the output current "i2" can be extracted and analysed. The parameters will be changed for the inductances and coupling coefficient simulating change in the relative position of the coils during operation. From the SINTEF prototype IPT-system measurements were taken, and are now used to analyse how the transfer function change as parameters are changed. In Table 5.1 only the parameter which depends on the relative distance of the coils are listed. The system frequency is kept at 5 kHz which also makes all the angular frequencies stay constant during changes of coil distance. The coupling coefficient and the self-inductances are taken from the measurements done earlier, and multiplied with the constant k_f to compensate the reduced frequency of a real IPT-system, shown in Appendix B.

Table 5.1 shows the parameters used for each of the operating distances considered in this thesis.

Parameter	d=20mm	d=30mm	d=40mm	d=45mm	d=50mm	d=60mm
System frequency (f)	5 kHz	5 kHz	5 kHz	5 kHz	5 kHz	5 kHz
Coupling coefficient (k)	0.611	0.4610	0.3470	0.3010	0.2620	0.2010
Primary inductance (L_1)	819.00µH	750.0µH	717.40µH	708.60µH	701.60µH	693.60µH
Secondary inductance (L_2)	534.80µH	490.0µH	468.80µH	463.00µH	428.80µH	454.00µH
Mutual inductance (M)	404.4µH	279.47µH	201.24µH	172.41µH	148.65µH	112.79µH
Primary capacitor (C_1)	1.237µF	1.3509µF	1.4123µF	1.4299µF	1.4441µF	1.4608µF
Secondary capacitor (C_2)	1.8965µF	2.0698µF	2.1634µF	2.1906µF	2.2106µF	2.2340µF

5.1 Linearization of the nonlinear averaged model

The linearization of the averaged model is done in MatLab with minor help from Simulink simulation to locate equilibrium points to define the operating point of the linearization. The operating point depends on what distance or value of coupling coefficient that is used, which is why five scripts are made to define the parameters and the operating point at each position of the coils. From Appendix the distances chosen is 20mm, 30mm, 40mm, 50mm and 60mm, all of them with no further misalignment. Initially, from the specialization project, the system frequency was set to 100 kHz, but this high frequency results in massive switching losses with

the current transistor technology. That is why the frequency is now set to 5 kHz that led to modifications to the measured self-inductances L1 and L2 by multiplying them with the factor $Kf = 20$ as defined in chapter 3.1.

In order to easily be able to change between the different operation distances, several Scripts define the parameters for each of the six cases. The parameters that changes as the operation distance is changed are marked in red. The parts of the script that is highlighted in light blue define the step changes of the inputs of the models, where step1 to step 3 define at what simulation time the step changes happen and "*deltax*" defines the amplitude of the changes:

$$step1 = u_1 * deltax, \quad step2 = \frac{u_1}{deltax^2} \quad and \quad step3 = u_1 * deltax \tag{5.1}$$

Script used to define parameters before the general linearization script is run:

```
%Basic system parameters and calculated values based on well-known formulas
f=5000
ws=2*pi*f
k=0.201
L1=(34.68e-6)*(100000/f)
L2=(22.70e-6)*(100000/f)
R1=1.5
R2=1.5
M=k*sqrt(L1*L2)
C2=1.001/(ws^2*L2)
C1=1/(ws^2*L1)
Lsigma1=L1-(M^2)/L2
Lsigma2=L2-(M^2)/L1
w1=1/sqrt(L1*C1)
w2=1/sqrt(L2*C2)
y=0
step1=0.015        %first step change happens after 0.015 seconds of simulation
step2=0.02         %second step change happens 0.015 seconds into the simulation
step3=0.025        %third step change happens 0.015 seconds into the simulation
deltax=0.90;       %defines the magnitude of the change in the step inputs

% operation point taken from simulation of the averaged model
X1=0.008819;
X2=0.0007968;
X3=0.00289;
X4=-1.572;
%inputs
u1=1.0;
u2=1.0;
```

The method that is used to extract the transfer function between $_1$ and i_2

1. Choose what distance the system is run in, and run the script with the correlated parameters.
2. Run the general linearization script, shown in Appendix C: Matlab scripts, which performs the following steps:

a. Define the state vectors, and the matrices and their functions.
b. Solving the matrices A, B, C and D numerically by inserting the values of the state variables from the given operating point.
c. Transforming from state space representation to transfer function representation, makes it possible to extract the wanted transfer function.
d. The transfer function between the input voltage and output current is negative because the output current is originally defined in the opposite direction of the current flow. A positive transfer function is preferable, so the current direction has been redefined to the opposite direction compared to Figure 4.1.
e. The positive transfer function is then analyzed by locating all the poles and zeroes that can be plotted in the S-plane.
f. Additionally a Bode plot and step plot is drawn to extract more information about the system.
g. The plots are being held to be able to compare the IPT-system's behaviour at different coupling coefficients. The different cases are color coded.

The transfer functions have been listed in Table 5.2 according to the relative distance between the coils when the measurements of the inductances were taken. MatLab originally presented the transfer functions with unnecessarily large coefficients in each term. To simplify, both the numerator and the denominator have been divided with the lowest common coefficient of the transfer function, which are the third order term in the numerator. The color code that is used for every plot is also shown in Table 5.2.

Table 5.2 shows the transfer functions for each of the six operation distances and tells the pole composition and the color code.

Distance	Resulting transfer function	Poles	Color code
60mm	$G_{60}(s) = \frac{s^3 + 1.414e07\,s^2 + 1.457e11\,s + 2.774e14}{10.98\,s^4 + 1.54e05\,s^3 + 7.361e08\,s^2 + 2.168e12\,s + 2.862e15}$	2 complex and 2 real	Magneta
50mm	$G_{50}(s) = \frac{s^3 + 8.844e07\,s^2 + 9.089e11\,s + 2.28e15}{48.87\,s^4 + 7.178e05\,s^3 + 4.357e09\,s^2 + 1.575e13\,s + 2.899e16}$	2 complex and 2 real	Blue
45mm	$G_{45}(s) = \frac{s^3 + 9.244e07\,s^2 + 9.659e11\,s + 2.824e15}{41.93\,s^4 + 6.487e05\,s^3 + 4.6e09\,s^2 + 1.842e13\,s + 4.064e16}$	4 complex	Black
40mm	$G_{40}(s) = \frac{s^3 + 9.818e07\,s^2 + 1.051e12\,s + 3.61e15}{35.62\,s^4 + 5.927e05\,s^3 + 5.053e09\,s^2 + 2.234e13\,s + 5.95e16}$	4 complex	Green
30mm	$G_{30}(s) = \frac{s^3 + 1.187e08\,s^2 + 1.337e12\,s + 6.377e15}{25.09\,s^4 + 5.157e05\,s^3 + 6.989e09\,s^2 + 3.649e13\,s + 1.423e17}$	4 complex	Cyan
20mm	$G_{20}(s) = \frac{s^3 + 1.689e08\,s^2 + 1.965e12\,s + 1.304e16}{16.45\,s^4 + 4.801e05\,s^3 + 1.253e10\,s^2 + 7.278e13\,s + 4.146e17}$	4 complex	Red

5.1.1 The importance of second order approximation

The transfer functions of the system are all fourth order transfer functions. The problem with higher order systems is that there is no analytical expressions for the parameters giving the information we need to design an optimal controller. This is why being able to derive a working second order approximation is essential when working with control systems. Second order systems are well equipped with analytical expressions for almost any parameter needed to evaluate the three design criteria explained in chapter 4.5.

5.2 Locating and analysing the poles and zeroes

From the transfer functions the zeroes and poles is found. They give most of the information about the system for an initial analysis. The first criterion is stability, which is ensured if all the poles are located in the left half plane of the S-plane. This implies that the real part of the pole is negative. Then, the poles and zeroes are tested against the rules of thumb in chapter 4.4 in order to simplify the transfer functions.

The zeroes and poles are listed in Table 5.3, where each parenthesis shows what value of s makes the transfer function yield zero and infinite respectively. The poles/zeroes that can be neglected/considered constant have orange font, while the poles and zeroes that may be cancelled against each other is given red font. When analysing the six transfer functions it seems that only the rules of thumb can be applied when the system is operated at low coupling coefficients ($k \leq 0.262$) that in this case only occurs in two of the operating distances (50mm and 60mm). At higher coupling coefficients new complex poles and zeroes is introduced, which reduce the chances of finding a valid second order approximation.

Table 5.3 lists the values of *s* that yields zeroes and poles.

Distance	Zeroes	Poles	Comments
60mm	(1.4133×10^7), (7791.7), (2518.8)	$(1514.1 + j3108.9), (1514.1 - j3108.9)$, (2595.7), (8393.8)	Possibly pole cancelling and neglection of zeroes and poles far from the dominating poles
50mm	(8.8434×10^7), (5928.5), (4348.8)	$(1740 + j4011.3), (1740 + j4011.3)$, (6221.6), (4987.3)	Possibly pole cancelling and neglection of zeroes and poles far from the dominating poles
45mm	(9.2428×10^7), $(5225.1 + j1802.8)$, $(5225.1 - j1802.8)$	$(1987 + j4543.5), (1987 - j4543.5)$ $(5748.4 + j2524.8), (5748.4 - j2524.8)$	Additional complex zeroes and poles
40mm	(9.8173×10^7), $(5354.4 + j2846.3)$, $(5354.4 - j2846.3)$	$(2419.9 + j5031.6), (2419.9 - j5031.6)$ $(5900.2 + j4333.1), (5900.2 - j4333.1)$	Additional complex zeroes and poles

30mm	$(1.1867 \times 10^8), (5634.3 + j4689.8), (5634.3 - j4689.8)$	$(2962.2 + j5264), (2962.2 - j5264)$ $(7315.4 + j10094), (7315.4 - j10094)$	Additional complex zeroes and poles
20mm	$(1.6891 \times 10^8), (5817.6 + j6582.8), (5817.6 - j6582.8)$	$(2935.3 + j5892.6), (2935.3 - j5892.6)$ $(11660 + j21112), (11660 + j21112)$	Additional complex zeroes and poles

From the transfer functions in Table 5.2 the zeroes and poles have been located and are plotted in the S-plane in Figure 5.1 and Figure 5.2. They are shown in two separate plots to be more comprehensive, as the markers in the MatLab scatterplot is hard to enlarge.

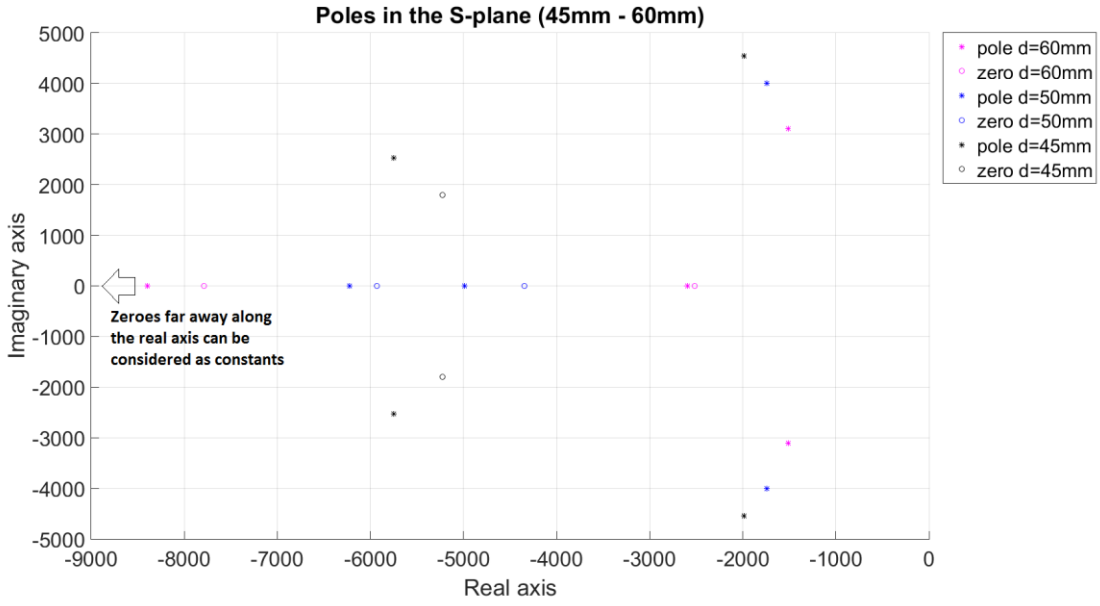

Figure 5.1 shows the poles and zeroes of the transfer functions: 45mm, 50mm and 60mm

When analyzing the location of the poles and zeroes of the transfer functions, it was discovered that the transfer functions with lowest coupling coefficient (d=50mm and d=60mm) was different from the cases with higher coupling coefficient (less air gap). The dominating poles are a complex pair for every transfer function, but the remaining poles and zeroes are only present along the real axis for the cases: d=50mm and d=60mm. This makes it much more likely that a second order approximation can be made for those transfer functions. For the other transfer functions, the third and fourth pole also make a complex pole pair, which makes it less likely that a second order approximation is possible. Additionally, two of the three zeroes of the small air gap transfer functions are complex, which also makes a second order approximation less likely to be valid.

The third zero of every transfer function is located several magnitudes away down the real axis from the dominating poles, and can simply be considered as constants. The other zeroes also might either be far enough from the dominating poles or able to cancel a pole. This needs to be tested by plotting Bode- and step plots of the original transfer functions and compare with a second order approximation.

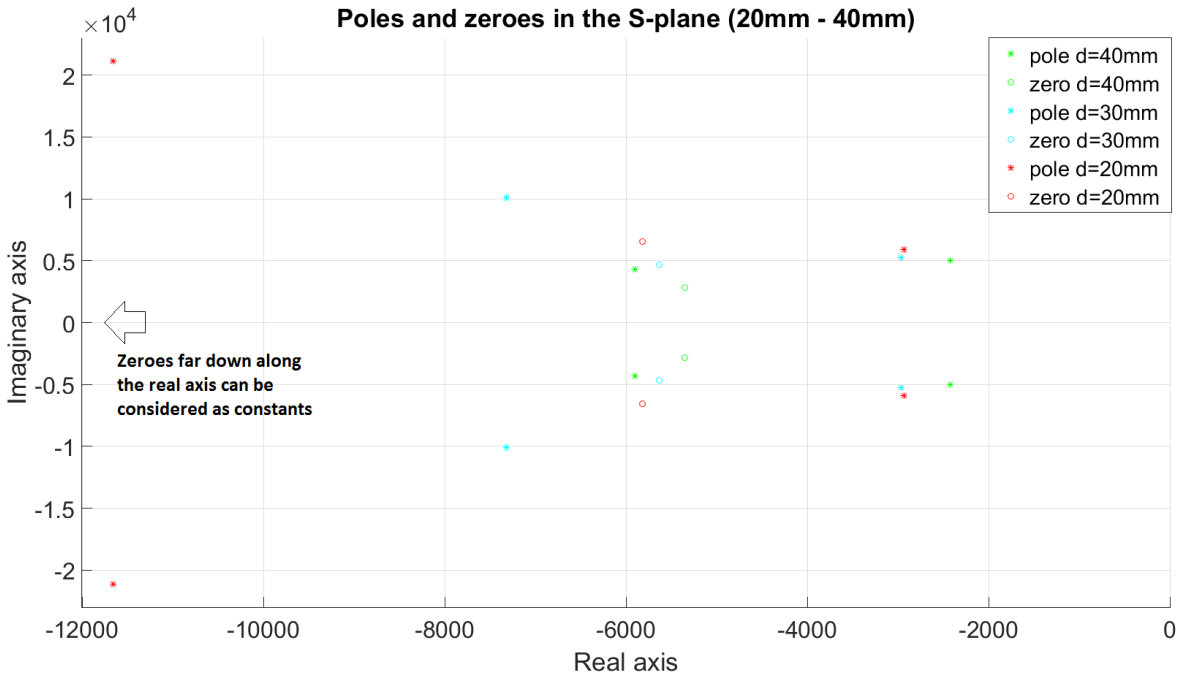

Figure 5.2 shows the poles and zeroes of the transfer functions: 20mm, 30mm and 40mm

Some trends on how the poles and zeroes change as the coupling changes can be observed in Figure 5.1 and Figure 5.2.

- The dominating poles become further away from origin as distance is decreased, both the real and imaginary part increases (exception at 30mm, which is closer to origin than at 20mm)
- The zeroes and the other poles are also located further from the origin as the distance between the coils increase, and at a certain distance (between 45mm and 50mm in this case) the two of the real zeroes and two of the real poles becomes complex poles.
- It seems like a lower coupling coefficient makes a second order approximation more plausible.

5.3 Verification of the second order approximations

The analysis of the zeroes and poles shows that as the coupling gets stronger, the accuracy of a second order approximation declines. As a verification method, the bode plots of three operation

distances has been compared to their second order approximations. The distances chosen are the smallest air gap, the widest air gap and the 45mm air gap case.

The procedure used to make a second order approximation of the system is to neglect poles that are far away from the dominating poles in the left half plane. Additionally the zeroes that are further left than the dominating poles will be considered as constants. Additionally, poles and zeroes which are close are cancelling each other out. The numerator of the approximation thus becomes a constant "K" and the denominator only consists of the dominating poles of the original transfer function. As an example, the transfer function of the widest air gap can be simplified.

$$G_{60}(s) = \frac{s^3 + 1.414\text{e}07\, s^2 + 1.457\text{e}11\, \text{s} + 2.774\text{e}14}{10.98\, s^4 + 1.54\text{e}05\, s^3 + 7.361\text{e}08\, s^2 + 2.168\text{e}12\, \text{s} + 2.862\text{e}15} \approx \frac{K}{10.98 * (s + 1514.1 + j3108.9)(s + 1514.1 - j3108.9)}$$

Where:

$$K = \lim_{s\to 0} G_{60}(s) * \lim_{s\to 0}(10.98\,(s + 1514.1 + j3108.9)(s + 1514.1 - j3108.9))$$

When calculating the equivalent constant "K" the simple method is to divide the constant term of the numerator original transfer function with the constant denominator, and then multiply it with the constant term introduced by the poles in the second order approximation. The resulting transfer function is:

$$G_{60}(s) \approx \frac{1.159e06}{s^2 + 3028s + 1.196e07}$$

When the second order approximation is made, it is plotted as a Bode plot in the same figure as the Bode plot of the original transfer function to compare and judge the accuracy of the approximation. The same comparison is also done with a step response plot created by a basic MatLab command.

5.3.1 Comparison of $G_{60}(s)$ and its second order approximation

Figure 5.3 and Figure 5.4 are both used to determine the validity of the second order approximation of the transfer function of the widest air gap:

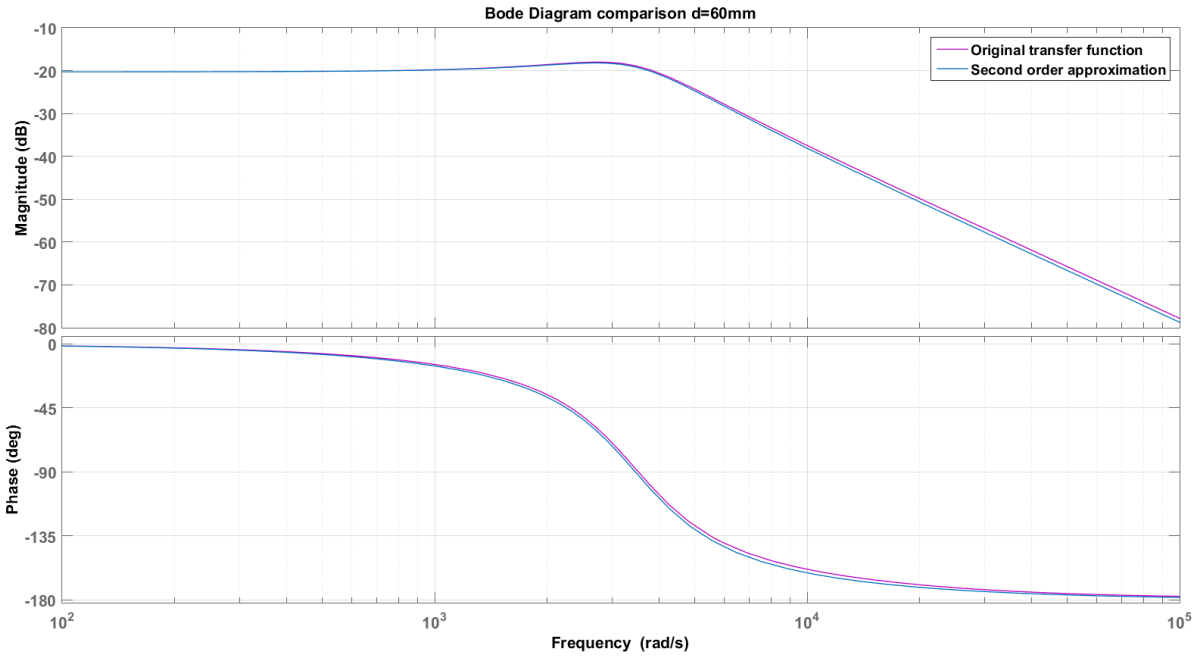

Figure 5.3 shows a comparison of the Bode plots of the original transfer function and its second order approximation for the operation distance of 60mm

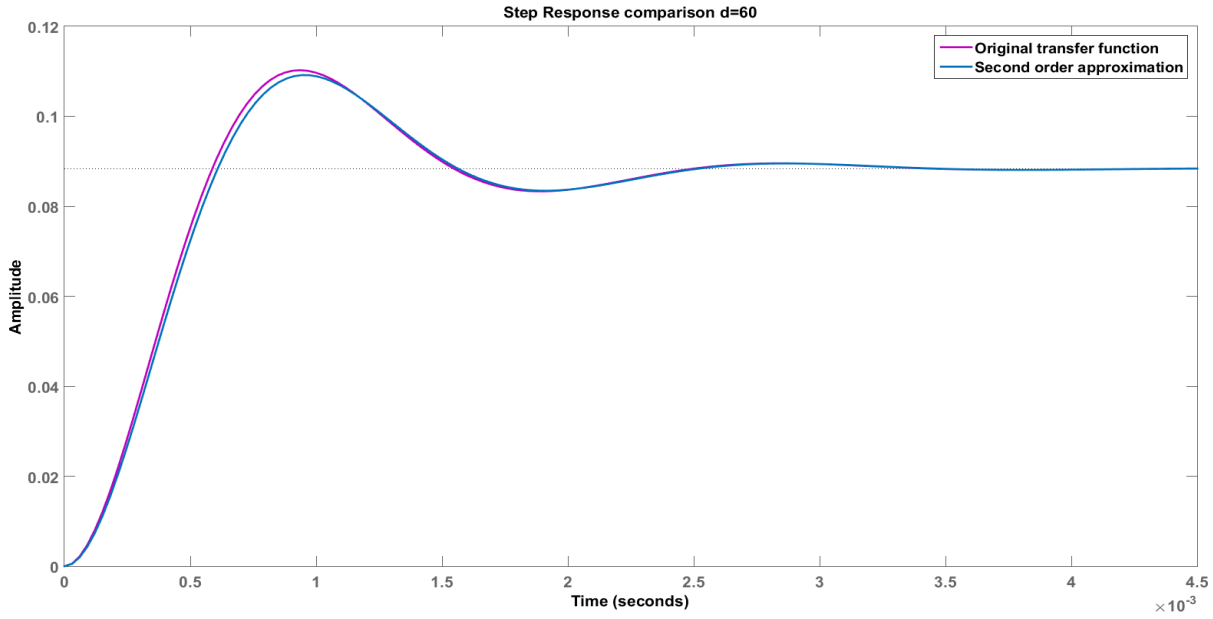

Figure 5.4 shows a comparison of the "closed loop step responses" of the original transfer function and its second order approximation for the operation distance of 60mm

From the plots shown in Figure 5.3 and Figure 5.4, the second order approximation is as expected very close to the original transfer function at widest air gap. The second order approximation seems to give slight underestimations of the magnitude, the phase in the Bode plot, and also underestimates the first peak in the step response plot. The approximation is not perfect, but it is close enough to be considered valid. This means that for low coupling coefficients a controller may be designed by using well known design methods based on second order systems.

5.3.2 Comparison of $G_{45}(s)$ and its second order approximation

Figure 5.5 and Figure 5.4 are both used to determine the validity of the second order approximation of the transfer function of the widest air gap. The approximation is expected to be less accurate because additional complex poles are present.

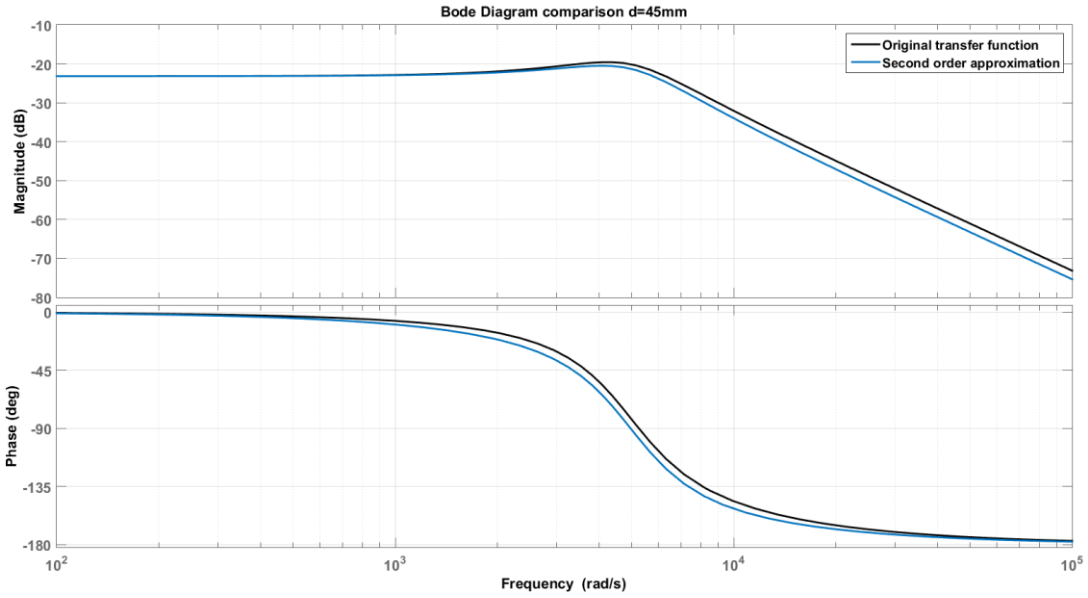

Figure 5.5 shows a comparison of the Bode plots of the original transfer function and its second order approximation for the operation distance of 45mm

The second order approximation of the medium air gap is even less accurate, as was expected when additional complex poles are present. The Bode plot in Figure 5.5 shows that the secondary approximation is similar to $G_{45}(s)$, but less accurate. From the step response plot in Figure 5.4, it is larger deviations between the approximation and the original transfer function. Although the approximation is beginning to deviate more as the coupling coefficient increase, it can be used as a coarse first design of a controller. For this system the borderline between a good enough second order approximation and an invalid approximation is found at a coupling coefficient around: $k = 0.30$.

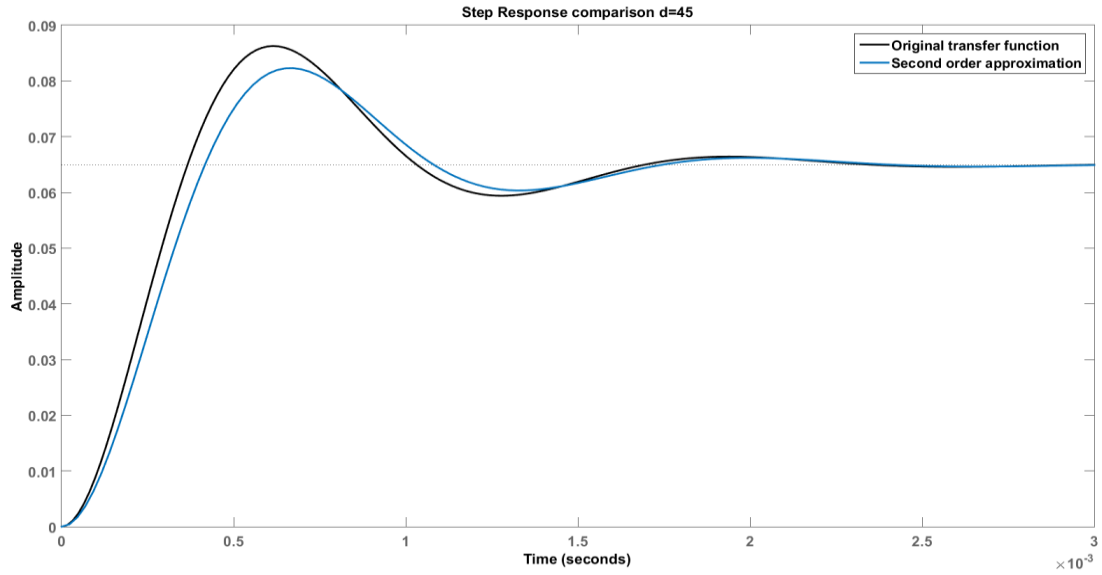

Figure 5.6 shows a comparison of the "closed loop step responses" of the original transfer function and its second order approximation for the operation distance of 45mm

5.3.3 Comparison of $G_{20}(s)$ and its second order approximation

Figure 5.7 and Figure 5.8 are both used to determine the validity of the second order approximation of the transfer function of the medium wide air gap.

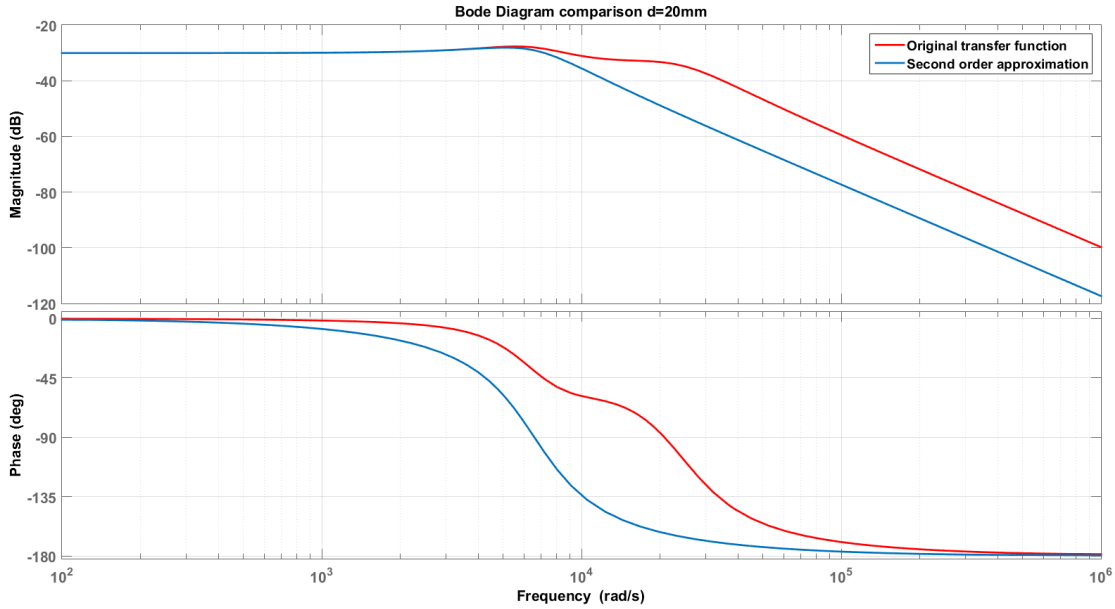

Figure 5.7 shows a comparison of the Bode plots of the original transfer function and its second order approximation for the operation distance of 20mm

The analysis of the poles and zeroes indicates that this approximation is much less accurate as additional complex poles with a huge imaginary component are present. This is verified in Figure 5.7 and Figure 5.8 since the second order approximation severely deviates from the original transfer function "$G_{20}(s)$". It is obviously not acceptable to model the transfer function of the smallest air gap with a second order approximation. The additional complex poles and zeroes have too heavy impact to be ignored.

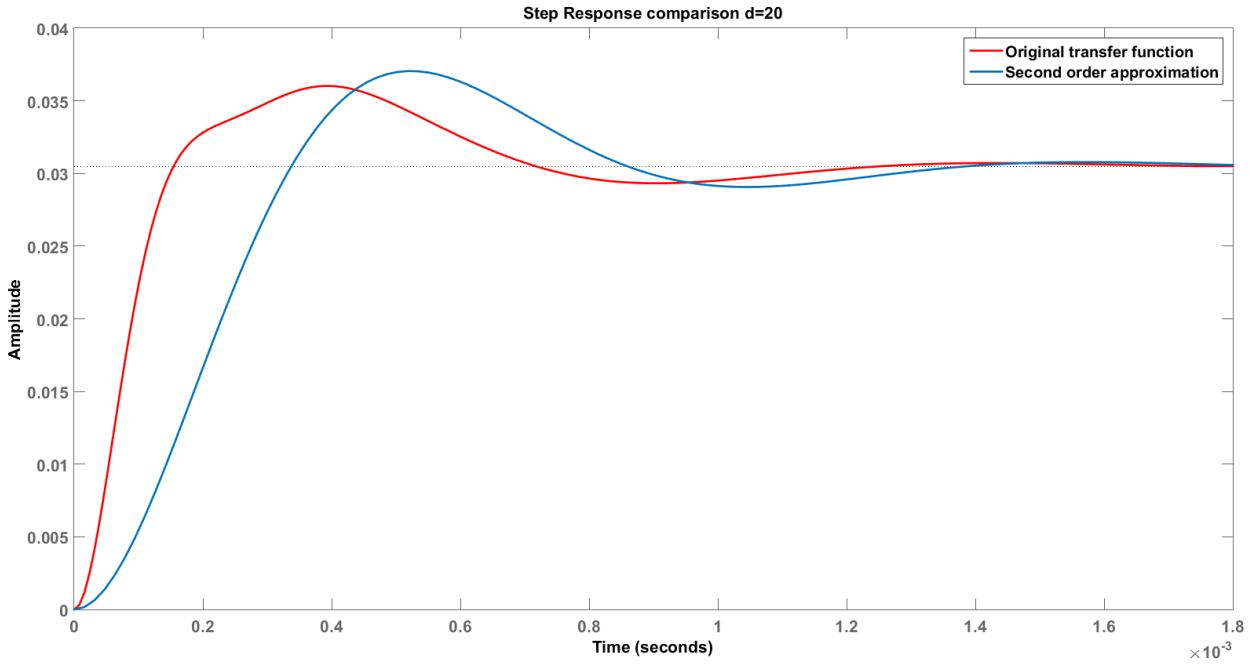

Figure 5.8 shows a comparison of the "closed loop step responses" of the original transfer function and its second order approximation for the operation distance of 20mm

The evaluation of whether the second order approximation to model the fourth order IPT-system is valid or not, depending on the coupling coefficient, is summarized in Table 5.4. The grading system used ranges from very good to very bad, where very good is almost identical and very bad is very large deviation. The intermediate steps are the following: good, fairly good, quite bad and bad. Fairly good is considered the borderline between whether the deviation is too great to accept or is acceptable. The other intermediate transfer functions ($G_{50}(s)$, $G_{40}(s)$ and $G_{30}(s)$) are assumed to fall in between the extremities. By running the MatLab script for the other transfer functions, this assumption has been confirmed, see Appendix D.

Table 5.4 shows the summary of how well the second order approximation is representing their original transfer functions.

Transfer function	Coupling coefficient	Magnitude (Bode plot)	Phase (Bode plot)	Step response	Verdict
$G_{60}(s)$	0.201	Very good	Very good	Good	Valid
$G_{50}(s)$	0.262	Good	Good	Fairly good	Valid
$G_{45}(s)$	0.301	Fairly good	Fairly good	Less good	Barely valid
$G_{40}(s)$	0.347	Quite bad	Quite bad	Bad	Not valid
$G_{30}(s)$	0.461	Bad	Bad	Very bad	Not valid
$G_{20}(s)$	0.611	Very bad	Very bad	Very bad	Not valid

6 Design of a controller

The fact that the second order approximation is not valid for all the cases means the design procedure for the controller must be divided into two. When the system is running at weak coupling, the controller steps may be designed by using common second order design methods. But as the air gap is reduced and the coupling coefficient is increased, and a second order approximation might not be valid, other design methods must be used. One important tool that is based on heavy simulations is computer tools. A computer can solve higher order transfer functions by running thousands of simulations in quite a short time. The computer tool is only used as a second choice to cope with transfer functions that clearly cannot be modelled by a second order approximation.

6.1 Advanced computer tools: Control System Manager

One of the alternate methods is to use computer tools, such as the (siso) tool that is included in the MatLab 2015a and the simulation tool Simulink. Siso stands for single input, single output (SISO) controllers and is part of an app called Control System Designer. This app let you design controllers by using interactive Bode, root locus and Nichols graphical editors that allows for adding, modifying and removing controller poles, zeroes and gains. This tool makes it possible to quickly see the effects of adding poles, zeroes and gains because you can immediately see the Bode plot change as parameters are changed. The app may also offer automated PID, Linear-Quadratic Gaussian (LQG) and Internal Model Control (IMC) tuning. Analysis of controllers and systems, as well as an optimization-based tuning option is among the tasks that can be done using this computer tool.

To illustrate how simple it is to design the controller according to set design criteria a controller for $G_{20}(s)$ is designed using (SISO) tools. As seen from the Figure 5.7, the uncompensated system does not cross the 0dB line, which means the phase margin is infinite. Additionally, the phase never reaches -180˚, which gives infinite gain margin too. This means the system is very stable, but when the other design criteria are checked in Figure 5.8 it is evident that the IPT system needs compensation. The steady state error is huge and need to be taken care of by introducing a controller.

$$e_{steady\ state\ 20} = \lim_{s\to 0} \frac{1}{1+G_{20}(s)} = \frac{1}{1+\frac{1.304e16}{4.146e17}} = 0.9695 \tag{6.1}$$

As a first step to design a controller, a desired value for the parameters describing the three design criteria are chosen. Phase margin and gain margin describes the stability of the system, if

either the gain or phase margin is zero or negative the system is unstable. The phase margin does also reflect the degree of damping in the system. To have good margins and ensuring stability the phase margin is desired to be around 55˚ and the gain margin over 15dB. Because of the high frequency of the system, it seems the settling time is very fast even for the uncompensated system. For an IPT system, a settling time below one second is acceptable. The steady state error is very important to minimize, which ensures the IPT system works as intended. As a first estimate less than 1% is proposed. A comparison of the uncompensated system versus the desired design parameters is shown in Table 6.1.

Table 6.1 compares the design criteria of the uncompensated system with a PI compensated system.

Parameters	Desired	Uncompensated system	Comments
Phase margin	At least 55˚	Infinite	Steady state error is greatly increased
Gain margin	At least 15 dB	Infinite	
Stable system?	Yes	Yes	System is very robust
Settling time	Less than 1 second	1.3ms	System speed is good
Percent overshoot	Less than 20%	19%	can be improved
Steady state error	Less than 5%	97%	must be improved

According to the analysis of the uncompensated system the steady state error is huge and needs to be drastically reduced. The best method to reduce the steady state error is to introduce an integrator in the forward loop accompanied by a gain to control the phase and gain margins.

6.1.1 Design procedure using Control System Toolbox

The integrator and the gain can be designed using the Control System Toolbox app in MatLab.

The design procedure is very intuitive and simple:

1. Step 1 is to enter: “controlSystemDesigner('bode',Tfsys)” after the general linearization script is run and a bode plot will appear in a new window:

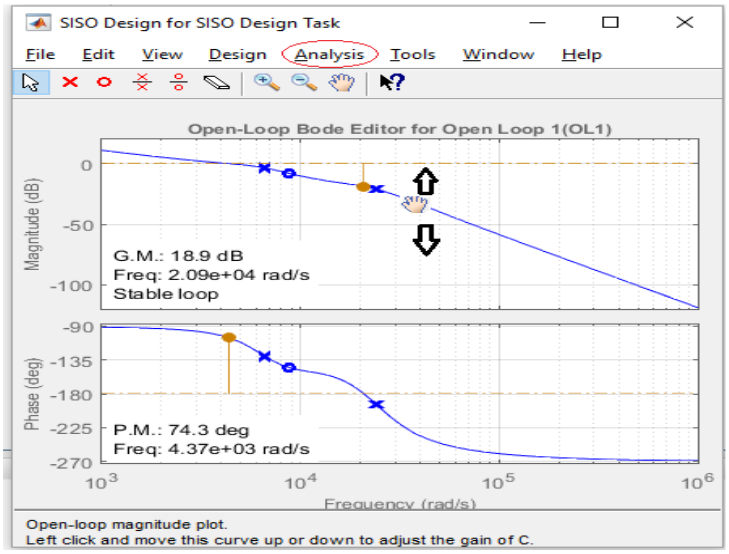

Figure 6.1 shows the Open-loop Bode Editor of the SISO toolbox, where Bode plots can be manipulated intuitively.

2. Open the analysis tag and select: “Response to step command”:

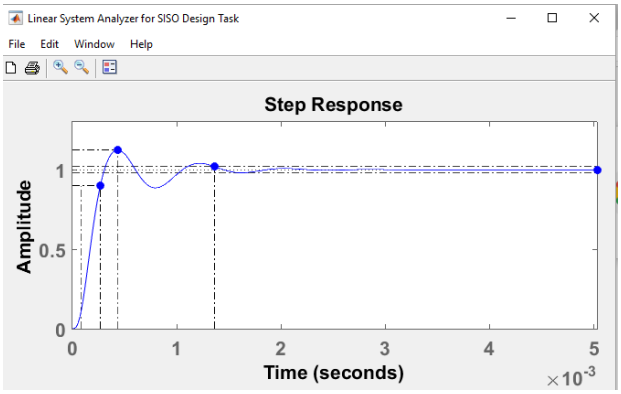

Figure 6.2 shows the related closed loop step response of the resulting compensated system.

3. Introduce a pole in the origin to add the integrator. Then, as indicated in Figure 6.1, the Bode plot itself can be moved with the cursor to obtain the desired phase margin.
4. For each selected phase margin, write down data from the step response and open the “Design” tab and select: edit compensator to find the current value of Ki.

The results, from testing an integrator with a gain in the forward loop at phase margins from 40˚ to 75˚, are shown in Table 6.2. The system seems to get better as the phase margin is increased, but the overshoot starts to occur on the second peak of the step response at around 65˚ phase margin, see Figure 6.3.

Table 6.2 shows how the controller gain (Ki) and the other parameter change as the phase margin is changed.

Phase margin	Integrator gain (Ki)	Gain margin	Settling time	Percent overshoot	Steady state error
40°	2.1894e+05	13dB	1.6ms	17%	Zero
45 °	1.8609e+05	14.4dB	1.35ms	13%	Zero
50 °	1.669e+05	15.4dB	1.4ms	10%	Zero
55 °	1.5558e+05	16dB	1.4ms	8%	Zero
60 °	1.3989e+05	16.9dB	1.4ms	5%	Zero
65 °	1.2886e+05	17.6dB	1.2ms	2.5%	Zero
70 °	1.2079e+05	18.2dB	1.2ms	1.5%	Zero
75 °	1.1124e+05	18.9dB	1.2ms	1%	Zero

This method to design a controller is very intuitive and yields great understanding of how the system reacts to different configurations of poles, zeroes and gains. Any compensator type can be selected, and by moving the Bode plot or the step response plot your specifications are met. This is a good first design phase to get to know the system and decide which controller is needed. The down side is the try and error part that makes it difficult to design a general controller that can cope with changing transfer functions depending on the operation of the IPT system.

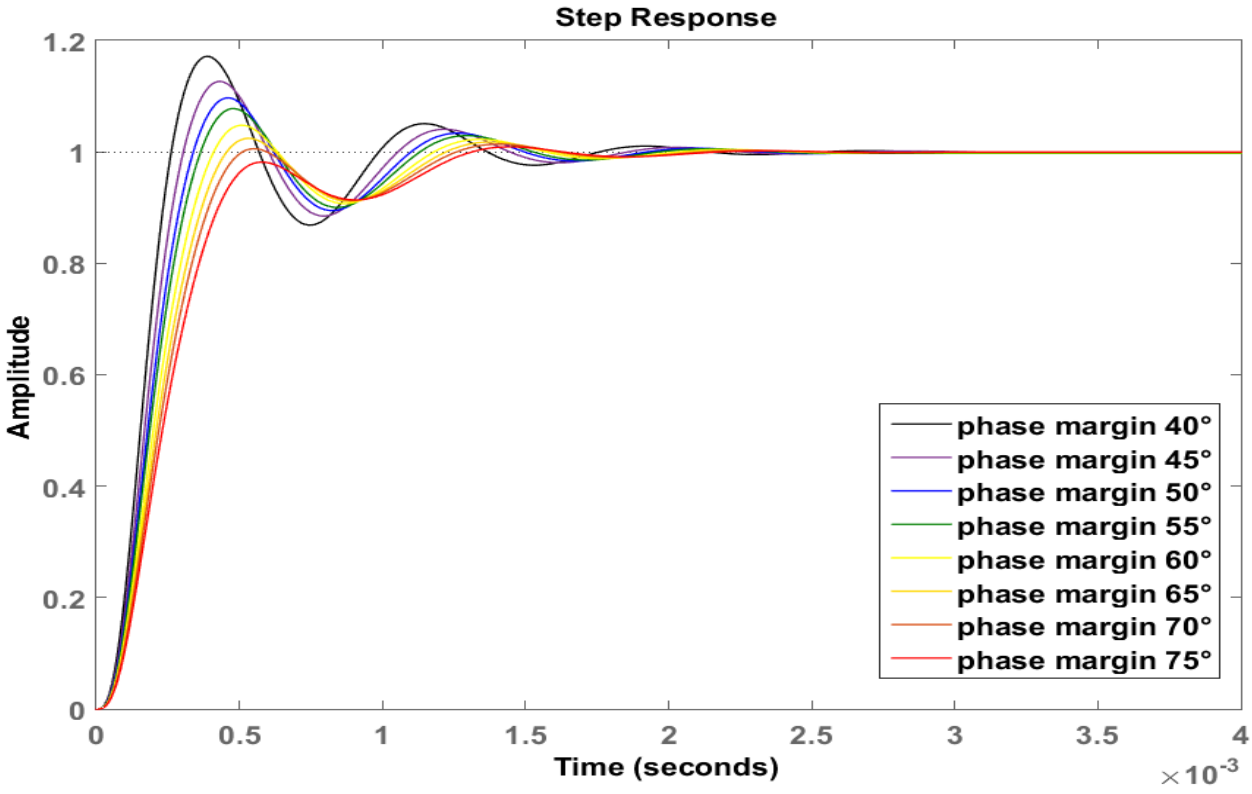

Figure 6.3 the resulting closed loop step responses of the compensated $G_{20}(s)$ as the phase margin is set to different values

Advanced computer tools could be used to design the controller for every possible configuration of the IPT-system, as the order of the system does not matter. The drawback is the inability to design the controller analytically. This means that the changes in the compensator, as the coupling coefficient change, is not possible to determine analytically. Thus, control design using computer tools may be less usable when designing a controller for the IPT system with variable coupling coefficient

7 Discussion

During the specialization project last autumn [15] I made the foundation of the averaged nonlinear time-invariant model, but during the process of writing this thesis an important error was found. The assumed system frequency was way too high to transfer the huge amounts of power that was intended. Thus, the model needed to adapt to a much lower frequency. The current frequency is set to 5kHz, which is one 20^{th} of the old system frequency. This change introduced new challenges when the measured inductances from the specialization project. To adapt the models two things had to be done:

- First, because inductance relies on the system frequency, the measured self-inductances were divided with the change of frequency ($K_f = 20$).
- Second, the step timings needed to be changed.

The system frequency of the measurements is not exactly 100kHz as assumed in the specialization project, but the measurements will still give the correct relationship between coupling coefficient and the distance between the coils. The measured self-inductances from the prototype can still be used to model a full-scale IPT system. This is because a change in the relative distance between the coils should change the self-inductances following the same relationship as the measured inductances.

5kHz might still give huge switching losses, but the purpose of this thesis is to explore the possibilities of designing a proper controller for a high power IPT-system. The current research on power electronics based on silicon carbide will enable IPT-systems to be run at higher frequencies. The increased frequency will increase the overall performance and efficiency of the system as well as reduce the physical size. It will be important to have established good controller designing methods to make IPT cheaper and better than cables. The modelling method used for describe the IPT is also an important research topic.

I believe the averaged, nonlinear time-invariant model based on CMT proposed by Hongchang et al. is a good way to model the basic IPT system. The calculations are complicated, but definitely manageable, and it seems to be a good model to base the control design on as the required information is kept. The model follows the amplitudes of the dynamic model, based on the basic differential equations of the mutually linked circuits, quite good for several configurations of the parameters. One thing I have had trouble with is to match the initial transients of the averaged model with the dynamic model, but the most important is the changes in inputs during operation. Another thing I have noticed is that the average model does not deal with sudden increase of the input, this problem is noticed whenever the initial conditions are set to low. This also happens if the step inputs of the model are set to drop down to zero and back up. I believe this happens because there is a limit of how quickly the average model can increase and still follow the

envelope. This should not pose any problem during normal operation of an IPT system, but it could pose a problem.

The linearization process has been gradually become more and more automatic as the scripts in Appendix C evolved. The transfer functions have been analysed, and much effort has gone to check for possible second order approximations for the fourth order transfer functions extracted from the linearized model. I have primarily only used the rules of thumb mentioned in chapter 4, but additional measures could potentially help achieving a valid second order approximation even for most of the small air gap transfer functions. By changing the values of the dominating poles, an approximation may be found even for some of the systems with additional poles. This method is hard to generalize, which is why I have not used it. This basic IPT system covered in this thesis does not represent every IPT system, by this I am trying to say that there is not certain IPT systems always gets impossible to apply second order approximation at higher coupling coefficient. I just observe that there is a correlation between the coupling coefficient and how well a general second order approximation describes the system. I also assume that there are IPT systems that cannot be approximated to a second order system for every coupling coefficient within its operation range. This is why I have proposed computer tools to be used for solving those higher order transfer functions, and possibly include the scripts and method used by the computer tool and utilize it when designing a controller.

When designing a controller for second order systems the procedures are well known, and the important parameters mostly have defined analytical expressions that can be utilized both in time domain as well as frequency domain. I have shown how the computer tool "(SISO) control design toolbox" in MatLab works, to explore how a system reacts to added poles, zeroes and gains, but I have not had the time to dig into the theory behind the computer tool. When designing a controller, I propose that the controller can be designed mainly by using second order approximations and use the well-established second order relationships to facilitate the control design greatly. But at the same time have a tool ready to deal with operation points of the IPT system that does not allow the transfer function to be represented by a second order approximation. From the analysis of poles and zeroes, it is clear that additional complex poles with large imaginary value in the vicinity of the dominating poles means the system cannot be approximated.

8 Conclusion

The future of wireless power transfer is exciting, and large improvements are possible as the power electronic technology is evolving. The averaged model based on "*coupled mode theory"* has been reliable when describing the basic IPT system. The model gives a graph that follows the transients quite well, and provides the needed information the system. One thing that could be improved is the capability to correctly react to large and sudden increase of the input signal.

The process of linearization of the averaged, nonlinear time-invariant model has been generalized to a good degree. Much effort has been put into making second order approximations of the resulting transfer functions to be able to use well established methods for controller design. The general rules used in this thesis have been proven to work on systems whose transfer function does not include large complex additional poles. However, it is possible to tune the location of the dominating poles to represent high order systems as second order approximations more accurately.

The design of a controller for this particular IPT system cannot solely be modeled by using second order control methods because of the large additional complex poles introduced at the smallest air gap. The second order design methods provide the best tools for handling design of a controller, but the IPT-system may not always be approximated for all coupling coefficients. This is why other methods also should be explored. This is why the usage of advanced computer tools is suggested as a good approach to handle the higher order transfer functions that cannot be approximated. The theory behind the computer tools should be further studied in order to more easily design controllers that can adapt to changes in the system transfer function according to the coupling of the coils.

For further work I propose to look more into the second order approximation to be able to represent more transfer functions as second order approximations. Additionally, the relationship between the coupling coefficient and how the poles and zeroes are located should be looked into. The averaged model based on coupled mode theory should also be further developed.

Bibliography

1. Davey, A. *Plugless at-A-glance*. 2015 [cited 2016; Available from: http://www.pluglesspower.com/wp-content/uploads/2015/11/PluglessAtAGlance.pdf.
2. Covic, G.A. and J.T. Boys, *Inductive Power Transfer.* Proceedings of the IEEE, 2013. **101**(6): p. 1276-1289.
3. Tesla, N., *The Transmission of Electric Energy Without Wires.* The Thirteenth Anniversary Number of the Electrical World and Engineer, 1904.
4. Systems Control Technology, I., *Roadway Powered Electric Vehicle Project Track Construction And Testing Program Phase 3D*. 1994.
5. Wärtsilä. *Wärtsilä and Cavotec to develop world's first marine wireless charging and mooring concept*. [Press release] 2016 [cited 2016 26.01]; Available from: www.wartsila.com/media/news/25-01-2016-wartsila-and-cavotec-to-develop-worlds-first-marine-wireless-charging-and-mooring-concept.
6. Barman, S.D., et al., *Wireless powering by magnetic resonant coupling: Recent trends in wireless power transfer system and its applications.* Renewable and Sustainable Energy Reviews, 2015. **51**: p. 1525-1552.
7. Dongwook, K., et al. *Propulsion and control of implantable micro-robot based on wireless power transfer*. in *Wireless Power Transfer Conference (WPTC), 2015 IEEE*. 2015.
8. Rim, C.T. and C.C. Mi, *Guest Editorial Special Issue on Wireless Power Transfer.* IEEE Transactions on Power Electronics, 2015. **30**(11): p. 6015-6016.
9. Li, H., et al., *A Maximum Efficiency Point Tracking Control Scheme for Wireless Power Transfer Systems Using Magnetic Resonant Coupling.* IEEE Transactions on Power Electronics, 2015. **30**(7): p. 3998-4008.
10. Hongchang, L., et al., *Dynamic Modeling Based on Coupled Modes for Wireless Power Transfer Systems.* Power Electronics, IEEE Transactions on, 2015. **30**(11): p. 6245-6253.
11. Guidi, G., *Wireless Transmission System for High Power Battery Charging*. 2014, SINTEF: Trondheim. p. 100 + appendices.
12. Kuphaldt, T.R., *Lessons in Electric Circuits*, in *Lessons in Electric Circuits*. 2000, Design Science Licence: www.allaboutcircuits.com.

13. Van Schuylenbergh, K.P., R., *Inductive Powering: Basic Theory and Application to Biomedical Systems*. 1st edition ed. 2009: Springer science.
14. Fotopoulou, K.a.F., Brian W., *Wireless Power Transfer in Loosely Coupled Links: Coil Misalignment Model.* IEEE Transactions on Magnetics publishes research in science and technology related to the basic physics and engineering of magnetism, magnetic materials, applied magnetics, magnetic devices, and magnetic data storage., 2011. **47**(2): p. 416-430.
15. Paulsen, L.J., *Wireless power transfer for marine and offshore applications*, in *Electrical engineering*. 2015, NTNU.
16. Zhang, W. and C. Mi, *Compensation Topologies for High Power Wireless Power Transfer Systems.* IEEE Transactions on Vehicular Technology, 2015. **PP**(99): p. 1-1.
17. Chwei-Sen, W., O.H. Stielau, and G.A. Covic, *Design considerations for a contactless electric vehicle battery charger.* Industrial Electronics, IEEE Transactions on, 2005. **52**(5): p. 1308-1314.
18. Tedeschi, E., *Control in inductive power transfer (IPT) systems* SINTEF, Editor. 2014.
19. Haus, H.A. and W. Huang, *Coupled-mode theory.* Proceedings of the IEEE, 1991. **79**(10): p. 1505-1518.
20. Nise, N.S., *Control Systems Engineering*. sixth edition ed. 2011: John Wiley & Sons (Asia) Pte Ltd. 903.
21. Packard, A. *ME 132 Feedback and Dynamic Systems*. 2002 [cited 2016 20.04.2016]; Class notes specifically for a subject in dynamic systems at berkely university]. Available from: https://jagger.berkeley.edu/~pack/me132/.

Appendix A

The model based on CMT befor it is averaged

$$\frac{d}{dt}a_1 = \omega_1 \cdot a_1 \cdot \sin\left(\omega_s t + \theta_1\right) \cdot \cos\left(\omega_s t + \theta_1\right)$$
$$- \frac{L_2 \cdot \sqrt{L_1} \cdot a_1 \cdot \cos\left(\omega_s t + \theta_1\right) \cdot \sin\left(\omega_s t + \theta_1\right)}{\sqrt{C_1} \cdot \left(L_1 \cdot L_2 - M^2\right)}$$
$$- \frac{L_2 \cdot R_1 \cdot a_1 \cdot \cos^2\left(\omega_s t + \theta_1\right)}{\left(L_1 \cdot L_2 - M^2\right)}$$
$$+ \frac{L_2 \cdot \sqrt{L_1} \cdot \cos\left(\omega_s t + \theta_1\right) \cdot sgn\left[\cos\left(\omega_s t\right)\right] \cdot v_1}{\sqrt{2} \cdot \left(L_1 \cdot L_2 - M^2\right)}$$
$$+ \frac{M \cdot R_2 \cdot \sqrt{L_1} \cdot a_2 \cdot \cos\left(\omega_s t + \theta_1\right) \cdot \cos\left(\omega_s t + \theta_2\right)}{\sqrt{L_2} \cdot \left(L_1 \cdot L_2 - M^2\right)}$$
$$+ \frac{M \cdot \sqrt{L_1} \cdot a_2 \cdot \cos\left(\omega_s t + \theta_1\right) \cdot \sin\left(\omega_s t + \theta_2\right)}{\sqrt{C_2} \cdot \left(L_1 \cdot L_2 - M^2\right)}$$
$$+ \frac{M \cdot \sqrt{L_1} \cdot \cos\left(\omega_s t + \theta_1\right) \cdot sgn\left[\cos\left(\omega_s t + \theta_2\right)\right] \cdot v_2}{\sqrt{2} \cdot \left(L_1 \cdot L_2 - M^2\right)}$$

$$\frac{d}{dt}a_1 = \omega_1 \cdot a_1 \cdot \sin\left(\omega_s t + \theta_1\right) \cdot \cos\left(\omega_s t + \theta_1\right)$$
$$+ \frac{\sqrt{\frac{L_1}{2}} \cdot \cos\left(\omega_s t + \theta_1\right)}{\left(L_1 \cdot L_2 - M^2\right)}$$
$$\times \left[- L_2 \cdot \sqrt{\frac{2}{C_1}} \cdot a_1 \cdot \sin\left(\omega_s t + \theta_1\right) \right.$$
$$- L_2 \cdot R_1 \sqrt{\frac{2}{L_1}} \cdot a_1 \cdot \cos\left(\omega_s t + \theta_1\right)$$
$$+ L_2 \cdot sgn\left[\cos\left(\omega_s t\right)\right] \cdot v_1$$
$$+ M \cdot R_2 \cdot \sqrt{\frac{2}{L_2}} \cdot a_2 \cdot \cos\left(\omega_s t + \theta_2\right)$$
$$+ M \cdot \sqrt{\frac{2}{C_2}} \cdot a_2 \cdot \sin\left(\omega_s t + \theta_2\right)$$
$$\left. + M \cdot sgn\left[\cos\left(\omega_s t + \theta_2\right)\right] \cdot v_2 \right]$$

$$\frac{d}{dt}\theta_1 = -\omega_s + \omega_1 - \omega_1 \cdot \sin^2(\omega_s t + \theta_1) + \frac{L_2 \cdot \sqrt{L_1} \cdot \sin^2(\omega_s t + \theta_1)}{\sqrt{C_1} \cdot (L_1 \cdot L_2 - M^2)} + \frac{L_2 \cdot R_1 \cdot \sin(\omega_s t + \theta_1) \cdot \cos(\omega_s t + \theta_1)}{(L_1 \cdot L_2 - M^2)} - \frac{L_2 \cdot \sqrt{L_1} \cdot \sin(\omega_s t + \theta_1) \cdot sgn[\cos(\omega_s t)] \cdot v_1}{a_1 \cdot \sqrt{2} \cdot (L_1 \cdot L_2 - M^2)} - \frac{M \cdot R_2 \cdot \sqrt{L_1} \cdot a_2 \cdot \sin(\omega_s t + \theta_1) \cdot \cos(\omega_s t + \theta_2)}{\sqrt{L_2} \cdot a_1 \cdot (L_1 \cdot L_2 - M^2)} - \frac{M \cdot \sqrt{L_1} \cdot a_2 \cdot \sin(\omega_s t + \theta_1) \cdot \sin(\omega_s t + \theta_2)}{\sqrt{C_2} \cdot a_1 \cdot (L_1 \cdot L_2 - M^2)} - \frac{M \cdot \sqrt{L_1} \cdot \sin(\omega_s t + \theta_1) \cdot sgn[\cos(\omega_s t + \theta_2)] \cdot v_2}{a_1 \cdot \sqrt{2} \cdot (L_1 \cdot L_2 - M^2)}$$

$$\frac{d}{dt}\theta_1 = -\omega_s + \omega_1 - \omega_1 \cdot \sin^2(\omega_s t + \theta_1) + \frac{\sqrt{\frac{L_1}{2}} \cdot \sin(\omega_s t + \theta_1)}{(L_1 \cdot L_2 - M^2) \cdot a_1} \times \left[L_2 \cdot \sqrt{\frac{2}{C_1}} \cdot a_1 \cdot \sin(\omega_s t + \theta_1) + L_2 \cdot R_1 \cdot \sqrt{\frac{2}{L_1}} \cdot a_1 \cdot \cos(\omega_s t + \theta_1) - L_2 \cdot sgn[\cos(\omega_s t)] \cdot v_1 - M \cdot R_2 \cdot \sqrt{\frac{2}{L_2}} \cdot a_2 \cdot \cos(\omega_s t + \theta_2) - M \cdot \sqrt{\frac{2}{C_2}} \cdot a_2 \cdot \sin(\omega_s t + \theta_2) - M \cdot sgn[\cos(\omega_s t + \theta_2)] \cdot v_2 \right]$$

$$\frac{d}{dt}a_2 = \omega_2 \cdot a_2 \cdot \sin(\omega_s t + \theta_2) \cdot \cos(\omega_s t + \theta_2) - \frac{L_1 \cdot \sqrt{L_2} \cdot a_2 \cdot \cos(\omega_s t + \theta_2) \cdot \sin(\omega_s t + \theta_2)}{\sqrt{C_2} \cdot (L_1 \cdot L_2 - M^2)} - \frac{L_1 \cdot R_2 \cdot a_2 \cdot \cos^2(\omega_s t + \theta_2)}{(L_1 \cdot L_2 - M^2) \cdot} - \frac{L_1 \cdot \sqrt{L_2} \cdot \cos(\omega_s t + \theta_2) \cdot sgn[\cos(\omega_s t + \theta_2)] \cdot v_2}{\sqrt{2} \cdot (L_1 \cdot L_2 - M^2)} + \frac{M \cdot R_1 \cdot \sqrt{L_2} \cdot a_1 \cdot \cos(\omega_s t + \theta_2) \cdot \cos(\omega_s t + \theta_1)}{\sqrt{L_1} \cdot (L_1 \cdot L_2 - M^2)} + \frac{M \cdot \sqrt{L_2} \cdot a_1 \cdot \cos(\omega_s t + \theta_2) \cdot \sin(\omega_s t + \theta_1)}{\sqrt{C_1} \cdot (L_1 \cdot L_2 - M^2)} - \frac{M \cdot \sqrt{L_2} \cdot \cos(\omega_s t + \theta_2) \cdot sgn[\cos(\omega_s t)] \cdot v_1}{\sqrt{2} \cdot (L_1 \cdot L_2 - M^2)}$$

$$\frac{d}{dt}a_2 = \omega_2 \cdot a_2 \cdot \sin(\omega_s t + \theta_2) \cdot \cos(\omega_s t + \theta_2) + \frac{\sqrt{\frac{L_2}{2}} \cdot \cos(\omega_s t + \theta_2)}{(L_1 \cdot L_2 - M^2)} \times \left[-L_1 \cdot \sqrt{\frac{2}{C_2}} \cdot a_2 \cdot \sin(\omega_s t + \theta_2) - L_1 \cdot sgn[\cos(\omega_s t + \theta_2)] \cdot v_2 + M \cdot R_1 \cdot \sqrt{\frac{2}{L_1}} \cdot a_1 \cdot \cos(\omega_s t + \theta_1) + M \cdot \sqrt{\frac{2}{C_1}} \cdot a_1 \cdot \sin(\omega_s t + \theta_1) - M \cdot sgn[\cos(\omega_s t)] \cdot v_1 \right]$$

$$\frac{d}{dt}\theta_2 = -\omega_s + \omega_2 - \omega_2\cdot\sin^2\left(\omega_s t + \theta_2\right) + \frac{L_1\cdot\sqrt{L_2}\cdot\sin^2\left(\omega_s t + \theta_2\right)}{\sqrt{C_2}\cdot\left(L_1\cdot L_2 - M^2\right)} + \frac{L_1\cdot R_2\cdot\sin\left(\omega_s t + \theta_2\right)\cdot\cos\left(\omega_s t + \theta_2\right)}{\left(L_1\cdot L_2 - M^2\right)} + \frac{L_1\cdot\sqrt{2}\cdot\sin\left(\omega_s t + \theta_2\right)\cdot sgn\left[\cos\left(\omega_s t + \theta_2\right)\right]\cdot v_2}{a_2\cdot\sqrt{2}\cdot\left(L_1\cdot L_2 - M^2\right)} - \frac{M\cdot R_1\cdot\sqrt{L_2}\cdot a_1\cdot\sin\left(\omega_s t + \theta_2\right)\cdot\cos\left(\omega_s t + \theta_1\right)}{\sqrt{L_1}\cdot a_2\cdot\left(L_1\cdot L_2 - M^2\right)} - \frac{M\cdot\sqrt{L_2}\cdot a_1\cdot\sin\left(\omega_s t + \theta_2\right)\cdot\sin\left(\omega_s t + \theta_1\right)}{\sqrt{C_1}\cdot a_2\cdot\left(L_1\cdot L_2 - M^2\right)} + \frac{M\cdot\sqrt{L_2}\cdot\sin\left(\omega_s t + \theta_2\right)\cdot sgn\left[\cos\left(\omega_s t\right)\right]\cdot v_1}{a_2\cdot\sqrt{2}\cdot\left(L_1\cdot L_2 - M^2\right)}$$

$$\frac{d}{dt}\theta_2 = -\omega_s + \omega_2 - \omega_2\cdot\sin^2\left(\omega_s t + \theta_2\right) + \frac{\sqrt{\frac{L_2}{2}}\cdot\sin\left(\omega_s t + \theta_2\right)}{\left(L_1\cdot L_2 - M^2\right)\cdot a_2} \times \left[L_1\cdot\sqrt{\frac{2}{C_2}}\cdot a_2\cdot\sin\left(\omega_s t + \theta_2\right) + L_1\cdot R_2\cdot\sqrt{\frac{2}{L_2}}\cdot a_2\cdot\cos\left(\omega_s t + \theta_2\right) + L_1\cdot sgn\left[\cos\left(\omega_s t + \theta_2\right)\right]\cdot v_2 - M\cdot R_1\cdot\sqrt{\frac{2}{L_1}}\cdot a_1\cdot\cos\left(\omega_s t + \theta_1\right) - M\cdot\sqrt{\frac{2}{C_1}}\cdot a_1\cdot\sin\left(\omega_s t + \theta_1\right) + M\cdot sgn\left[\cos\left(\omega_s t\right)\right]\cdot v_1\right]$$

$$\frac{d}{dt}a_1\ averaged = -\frac{L_2\cdot R_1\cdot a_1}{2\cdot\left(L_1\cdot L_2 - M^2\right)} - \frac{M\cdot\sqrt{L_1}\cdot a_2\cdot\sin\left(\theta_1 - \theta_2\right)}{2\cdot\sqrt{C_2}\cdot\left(L_1\cdot L_2 - M^2\right)} + \frac{M\cdot R_2\cdot\sqrt{L_1}\cdot a_2\cdot\cos\left(\theta_1 - \theta_2\right)}{2\cdot\sqrt{L_2}\cdot\left(L_1\cdot L_2 - M^2\right)} + \frac{\sqrt{2}\cdot L_2\cdot\sqrt{L_1}\cdot v_1\cdot\cos\left(\theta_1\right)}{\pi\cdot\left(L_1\cdot L_2 - M^2\right)} + \frac{\sqrt{2}\cdot M\cdot\sqrt{L_1}\cdot v_2\cdot\cos\left(\theta_1 - \theta_2\right)}{\pi\cdot\left(L_1\cdot L_2 - M^2\right)}$$

$$\frac{d}{dt}\theta_1\ averaged = -\omega_s + \frac{\omega_1}{2} + \frac{L_2\cdot\sqrt{L_1}}{2\cdot\sqrt{C_1}\cdot\left(L_1\cdot L_2 - M^2\right)} - \frac{M\cdot\sqrt{L_1}\cdot a_2\cdot\cos\left(\theta_1 - \theta_2\right)}{2\cdot\sqrt{C_2}\cdot a_1\left(L_1\cdot L_2 - M^2\right)} - \frac{M\cdot R_2\cdot\sqrt{L_1}\cdot a_2\cdot\sin\left(\theta_1 - \theta_2\right)}{2\cdot\sqrt{L_2}\cdot a_1\cdot\left(L_1\cdot L_2 - M^2\right)} - \frac{\sqrt{2}\cdot L_2\cdot\sqrt{L_1}\cdot v_1\cdot\sin\left(\theta_1\right)}{a_1\cdot\pi\cdot\left(L_1\cdot L_2 - M^2\right)} - \frac{\sqrt{2}\cdot M\cdot\sqrt{L_1}\cdot v_2\cdot\sin\left(\theta_1 - \theta_2\right)}{a_1\cdot\pi\cdot\left(L_1\cdot L_2 - M^2\right)}$$

$$\frac{d}{dt} a_2\ averaged = -\frac{L_1 \cdot R_2 \cdot a_2}{2 \cdot \left(L_1 \cdot L_2 - M^2\right)} + \frac{M \cdot \sqrt{L_2} \cdot a_1 \cdot \sin\left(\theta_1 - \theta_2\right)}{2 \cdot \sqrt{C_1} \cdot \left(L_1 \cdot L_2 - M^2\right)} + \frac{M \cdot R_1 \cdot \sqrt{L_2} \cdot a_1 \cdot \cos\left(\theta_1 - \theta_2\right)}{2 \cdot \sqrt{L_1} \cdot \left(L_1 \cdot L_2 - M^2\right)} - \frac{\sqrt{2} \cdot L_1 \cdot \sqrt{L_2} \cdot v_2 \cdot \cos(0)}{\pi \cdot \left(L_1 \cdot L_2 - M^2\right)} - \frac{\sqrt{2} \cdot M \cdot \sqrt{L_2} \cdot v_1 \cdot \cos\left(\theta_2\right)}{\pi \cdot \left(L_1 \cdot L_2 - M^2\right)}$$

$$\frac{d}{dt} \theta_2\ averaged = -\omega_s + \frac{\omega_2}{2} + \frac{L_1 \cdot \sqrt{L_2}}{2 \cdot \sqrt{C_2} \cdot \left(L_1 \cdot L_2 - M^2\right)} - \frac{M \cdot \sqrt{L_2} \cdot a_1 \cdot \cos\left(\theta_1 - \theta_2\right)}{2 \cdot \sqrt{C_1} \cdot a_2 \left(L_1 \cdot L_2 - M^2\right)} + \frac{M \cdot R_1 \cdot \sqrt{L_2} \cdot a_1 \cdot \sin\left(\theta_1 - \theta_2\right)}{2 \cdot \sqrt{L_1} \cdot a_2 \cdot \left(L_1 \cdot L_2 - M^2\right)} + \frac{\sqrt{2} \cdot M \cdot \sqrt{L_2} \cdot v_1 \cdot \sin\left(\theta_2\right)}{a_2 \cdot \pi \cdot \left(L_1 \cdot L_2 - M^2\right)}$$

Appendix B

Measured inductances from the SINTEF prototype

Measured misalignment			Self-inductance (Open loop)		Calculated M	Total inductance (inductance in series)		Calculated k	Control
d (mm)	x (mm)	y (mm)	L11 (µH)	L22 (µH)	(Lb-La)/4 (µH)	La (µH)	Lb (µH)	M/root(L11*L22)	
20.00	0.00	0.00	40.95	26.74	20.22	27.26	108.13	0.611	-0.005
25.00	0.00	0.00	38.86	25.38	16.70	30.79	97.59	0.532	0.05
30.00	0.00	0.00	37.50	24.50	13.96	34.05	89.90	0.461	0.025
35.00	0.00	0.00	36.54	23.86	11.80	36.79	84.00	0.400	0.005
40.00	0.00	0.00	35.87	23.44	10.06	39.16	79.38	0.347	0.04
45.00	0.00	0.00	35.43	23.15	8.63	41.32	75.84	0.301	0
50.00	0.00	0.00	35.08	22.94	7.44	43.23	72.97	0.262	-0.08
55.00	0.00	0.00	34.86	22.77	6.39	44.92	70.49	0.227	-0.075
60.00	0.00	0.00	34.68	22.70	5.65	46.13	68.74	0.201	-0.055
65.00	0.00	0.00	34.55	22.61	4.94	47.34	67.11	0.177	-0.065
70.00	0.00	0.00	34.41	22.53	4.35	48.35	65.74	0.156	-0.105
75.00	0.00	0.00	34.33	22.49	3.87	49.19	64.65	0.139	-0.1
80.00	0.00	0.00	34.29	22.46	3.42	50.02	63.69	0.123	-0.105
85.00	0.00	0.00	34.27	22.43	3.07	50.64	62.90	0.111	-0.07
90.00	0.00	0.00	34.25	22.43	2.72	51.29	62.17	0.098	-0.05
95.00	0.00	0.00	34.22	22.41	2.42	51.84	61.53	0.087	-0.055
100.00	0.00	0.00	34.18	22.39	2.19	52.28	61.02	0.079	-0.08
105.00	0.00	0.00	34.18	22.38	1.98	52.63	60.56	0.072	-0.035
110.00	0.00	0.00	34.16	22.37	1.78	53.06	60.17	0.064	-0.085
115.00	0.00	0.00	34.15	22.36	1.61	53.38	59.81	0.058	-0.085

120.00	0.00	0.00	34.14	22.37	1.47	53.64	59.52	0.053	-0.07
125.00	0.00	0.00	34.12	22.36	1.33	53.90	59.21	0.048	-0.075
130.00	0.00	0.00	34.11	22.36	1.21	54.11	58.96	0.044	-0.065
135.00	0.00	0.00	34.10	22.36	1.13	54.31	58.81	0.041	-0.1
140.00	0.00	0.00	34.10	22.37	1.03	54.53	58.63	0.037	-0.11
145.00	0.00	0.00	34.09	22.38	0.95	54.66	58.44	0.034	-0.08
150.00	0.00	0.00	34.09	22.38	0.86	54.84	58.29	0.031	-0.095

Appendix C: Matlab scripts

Default parameters for the IPT models and simulations

```
%Basic system parameters and calculated values based on well-known formulas
f=5000
ws=2*pi*f
k=0.262
L1=(35.08e-6)*(100000/f)
L2=(22.94e-6)*(100000/f)
R1=1.5
R2=1.5
M=k*sqrt(L1*L2)
C2=1.001/(ws^2*L2)
C1=1/(ws^2*L1)
Lsigma1=L1-(M^2)/L2
Lsigma2=L2-(M^2)/L1
w1=1/sqrt(L1*C1)
w2=1/sqrt(L2*C2)
y=0
step1=0.015
step2=0.02
step3=0.025
deltax=0.90;

%% The representation of the averaged model constants (term by term)
% A1 through A5 are the constants of d/dt(a1) sorted by term (top-bottom)
A1=L2*R1/(2*(L1*L2-M^2))
A2=M*sqrt(L1)/(2*sqrt(C2)*(L1*L2-M^2))
A3=M*R2*sqrt(L1)/(2*sqrt(L2)*(L1*L2-M^2))
A4=sqrt(2)*L2*sqrt(L1)/(pi*(L1*L2-M^2))
A5=sqrt(2)*M*sqrt(L1)/(pi*(L1*L2-M^2))

% B1 through B5 are the constants of d/dt(ø1) sorted by term (top-bottom)
B1=L2*sqrt(L1)/(2*sqrt(C1)*(L1*L2-M^2))
B2=M*sqrt(L1)/(2*sqrt(C2)*(L1*L2-M^2))
B3=M*R2*sqrt(L1)/(2*sqrt(L2)*(L1*L2-M^2))
B4=sqrt(2)*L2*sqrt(L1)/(pi*(L1*L2-M^2))
B5=sqrt(2)*M*sqrt(L1)/(pi*(L1*L2-M^2))

% a1 through a5 are the constants of d/dt(a2) sorted by term (top-bottom)
a1=(L1*R2)/(2*(L1*L2-M^2))
a2=(M*sqrt(L2))/(2*sqrt(C1)*(L1*L2-M^2))
a3=(M*R1*sqrt(L2))/(2*sqrt(L1)*(L1*L2-M^2))
a4=(sqrt(2)*L1*sqrt(L2))/(pi*(L1*L2-M^2))
a5=(sqrt(2)*M*sqrt(L2))/(pi*(L1*L2-M^2))

% b1 through b4 are the constants of d/dt(ø2) sorted by term (top-bottom)
b1=L1*sqrt(L2)/(2*sqrt(C2)*(L1*L2-M^2))
```

```
b2=M*sqrt(L2)/(2*sqrt(C1)*(L1*L2-M^2))
b3=M*R1*sqrt(L2)/(2*sqrt(L1)*(L1*L2-M^2))
b4=sqrt(2)*M*sqrt(L2)/(pi*(L1*L2-M^2))
%% The relationship between the constant terms and their state variables

% list of state variables in a format which can be used by the DEE block
x(1)=a1
x(2)=ø1
x(3)=a2
x(4)=ø2

%State 1 in correct format
-A1*x(1)-A2*x(3)*sin(x(2)-x(4))+A3*x(3)*cos(x(2)-x(4))
+A4*u(1)*cos(x(2))+A5*u(2)*cos(x(2)-x(4))

%Xo (initial condition)
0.001

%State 2 in correct format
-ws+w1/2+B1-B2*x(3)*cos(x(2)-x(4))/x(1)-B3*x(3)*sin(x(2)-x(4))/x(1)
-B4*u(1)*sin(x(2))/x(1)-B5*u(2)*sin(x(2)-x(4))/x(1)

%Xo (initial condition)
-pi/6

%State 3 in correct format
-a1*x(3)+a2*x(1)*sin(x(2)-x(4))+a3*x(1)*cos(x(2)-x(4))
-a4*u(2)-a5*u(1)*cos(x(4))

%Xo (initial condition)
0.001

%State 4 in correct format
-ws+w2/2+b1-b2*x(1)*cos(x(2)-x(4))/x(3)+b3*x(1)*sin(x(2)-x(4))/x(3)
+b4*u(1)*sin(x(4))/x(3)

%Xo (initial condition)
0
```

General linearization script:

```
%define parameters and vectors
x1 = sym('x1');
x2 = sym('x2');
x3 = sym('x3');
x4 = sym('x4');
u1 = sym('u1');
u2 = sym('u2');

x=  [x1; x2; x3; x4];
u= [u1; u2];

f1=-A1*x1-A2*x3*sin(x2-x4)+A3*x3*cos(x2-x4)+A4*u1*cos(x2)+A5*u2*cos(x2-x4);
f2=-ws+w1/2+B1-B2*x3*cos(x2-x4)/x1-B3*x3*sin(x2-x4)/x1-B4*u1*sin(x2)/x1-
B5*u2*sin(x2-x4)/x1;
f3=-a1*x3+a2*x1*sin(x2-x4)+a3*x1*cos(x2-x4)-a4*u2-a5*u1*cos(x4);
f4=-ws+w2/2+b1-b2*x1*cos(x2-x4)/x3+b3*x1*sin(x2-x4)/x3+b4*u1*sin(x4)/x3;

g1=1/pi*sqrt(2/L1)*x1*cos(x2);
g2=-1/pi*sqrt(2/L2)*x3;

%% differentiating resulting in the desired matrices to find the state space
model
F=[f1;f2;f3;f4];
fx=[diff(F,x1) diff(F,x2) diff(F,x3) diff(F,x4)];
fdu1=diff(F,u1);
fdu2=diff(F,u2);

dg1=[diff(g1,x1) diff(g1,x2) diff(g1,x3) diff(g1,x4)];
dg2=[diff(g2,x1) diff(g2,x2) diff(g2,x3) diff(g2,x4)];

%% Equilibrium point of current operation of IPT-system

x1=X1;
x2=X2;
x3=X3;
x4=X4;
u1=1.0;
u2=1.0;

%% Substituting the values of the state variables into the matrices and
simplfy
Fx= vpa(subs (fx), 50);
fdu= vpa (subs ([fdu1 fdu2]), 50);
dg= vpa (subs([dg1; dg2]), 50);
%% Here the matrices are just prepared for the Simulink model (not used
further)
digits(50)
A= double(Fx)
B= double(fdu)
C= double(dg)
D= [0 0; 0 0];
```

```
%% Transform between state space and transfer functions
I= eye(4);

s=sym('s');
As=s*I-Fx;
Gs=dg*inv(As)*fdu;
Tf=simplify (Gs)

%% extracting only the desired transfer function from "v1" to "i2"
[n,d]=numden(Tf(2,1));
[n,d]=numden(Tf(2,1));
num21=sym2poly (n);
den21=sym2poly(d);

Tf21=tf(num21,den21)

% Defining the output current to be positive by changing the defined
direction.
Tfsys=-Tf21

%% Information about the poles and zeroes of the positive transfer function.
Z= zero(Tfsys);
P= pole(Tfsys);
Yz = imag(Z).'
Xz = real(Z).'
Yp = imag(P).'
Xp = real(P).'


%% Scatter plot of the poles and zeroes of Tfsys
figure(1)
grid on
scatter(Xp,Yp,'*',i)
hold on
scatter(Xz,Yz,'o',i)

%setting proper axis limits
if any(max(Xp) > 0)
    xlim([1.1*min(Xp), 1.1*max(Xp)])
else
    xlim([1.1*min(Xp), 0]);
end
if any(max(Yp) > min(Yp) )
    ylim([1.1*min(Yp), 1.1*max(Yp)])
else
    ylim auto
end

%step response of the transfer function (color coded "i")
figure(2)
step(Tfsys,i);
hold on
% Bode plot of the transfer function (color coded "i")
figure(3)
```

```
grid on
Bode(Tfsys,i);
hold on
```

The script section that derives the second order approximations:

Script for d=60mm

```
%% Calculation of the second order approximation at d=60
(needs more work to be a general approach)
K=-num21(4)/den21(5)*(Xp(3)^2+Yp(3)^2)
s=sym('s')
zp = collect(simplify (K/((s-P(2))*(s-P(3)))))
[na,da]=numden(zp);
numa=sym2poly (na);
dena=sym2poly(da);
Tfapprox=tf(numa/dena(1),dena/dena(1))
Tfacl=feedback(Tfapprox,1)
Pa=pole(Tfapprox)
Za=zero(Tfapprox)
[r,p,k] = residue(numa, dena)
```

Script for d=45mm

```
%% Calculation of the second order approximation at d=45
(needs more work to be a general approach)
K=-num21(4)/den21(5)*(Xp(3)^2+Yp(3)^2)
s=sym('s')
zp = collect(simplify (K/((s-P(3))*(s-P(4)))))
[na,da]=numden(zp);
numa=sym2poly (na);
dena=sym2poly(da);
Tfapprox=tf(numa/dena(1),dena/dena(1))
Tfacl=feedback(Tfapprox,1)
Pa=pole(Tfapprox)
Za=zero(Tfapprox)
[r,p,k] = residue(numa, dena)
```

Appendix D

Evaluation of second order approximations:

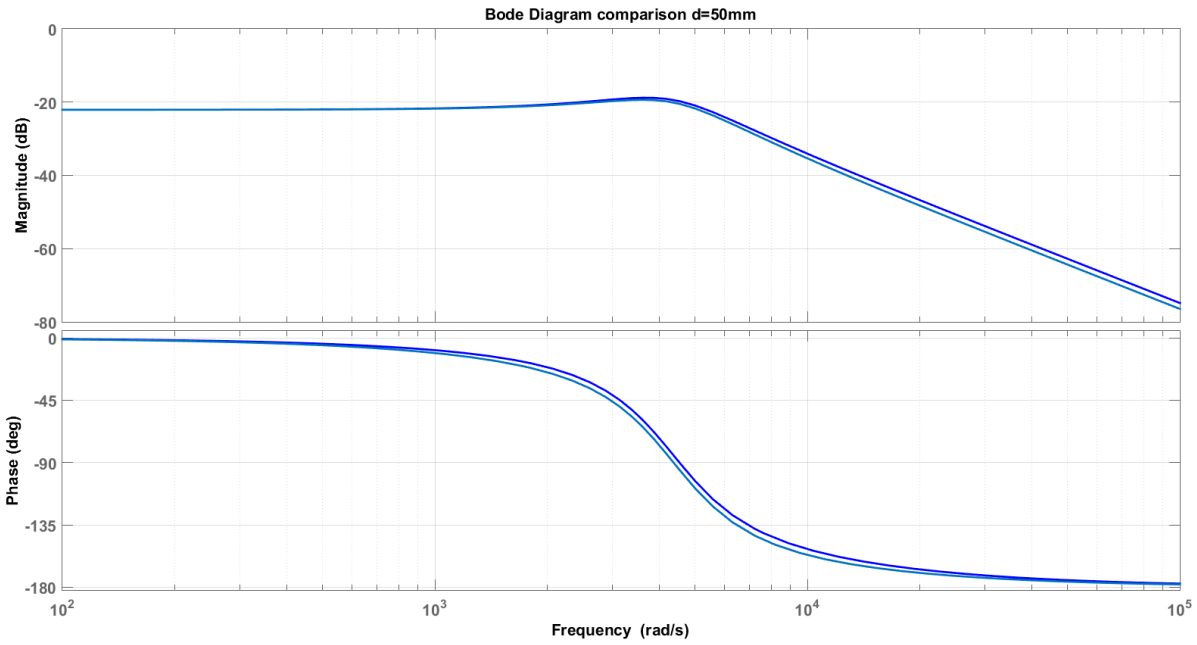

Figure D.1 shows a comparison of the Bode plots of the original transfer function and its second order approximation for the operation distance of 50mm

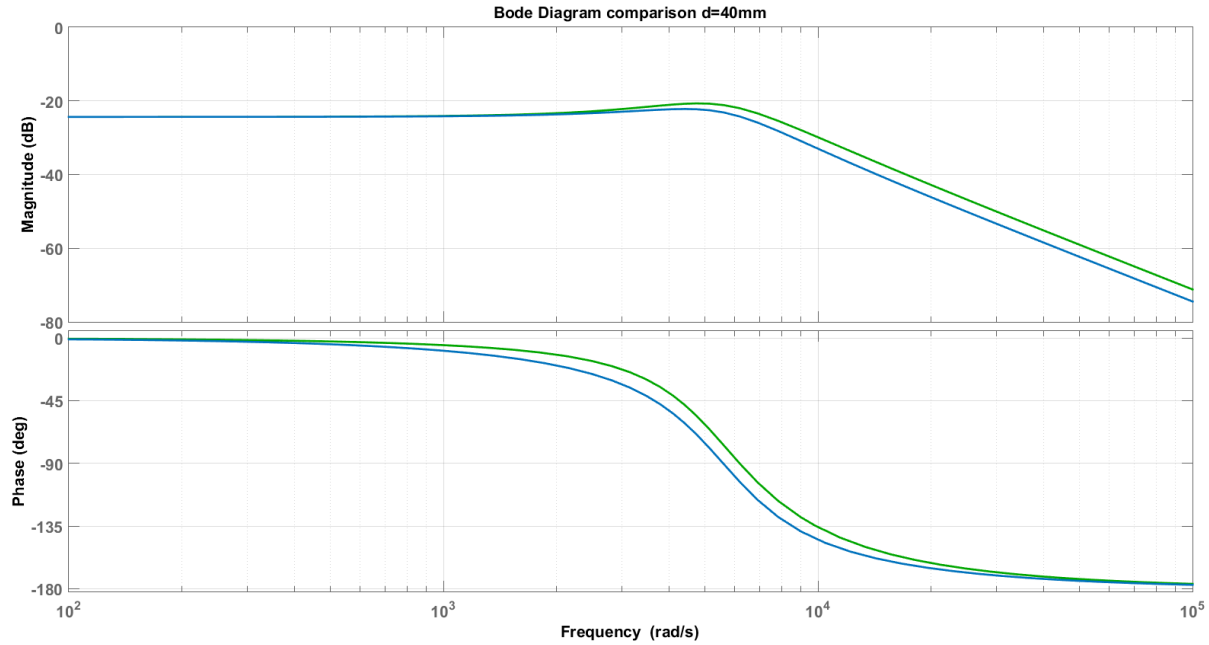

Figure D.2 shows a comparison of the Bode plots of the original transfer function and its second order approximation for the operation distance of 40mm

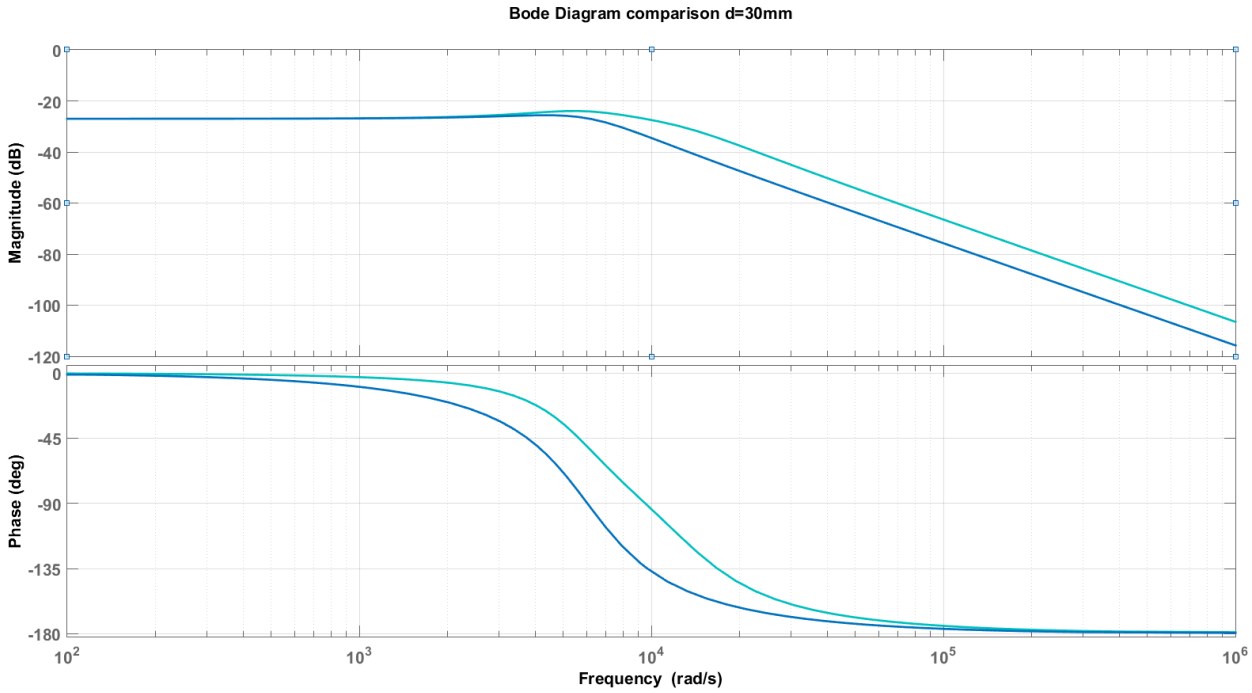

Figure D.3 shows a comparison of the Bode plots of the original transfer function and its second order approximation for the operation distance of 30mm

Bode plot and step response of the integrator compensated system

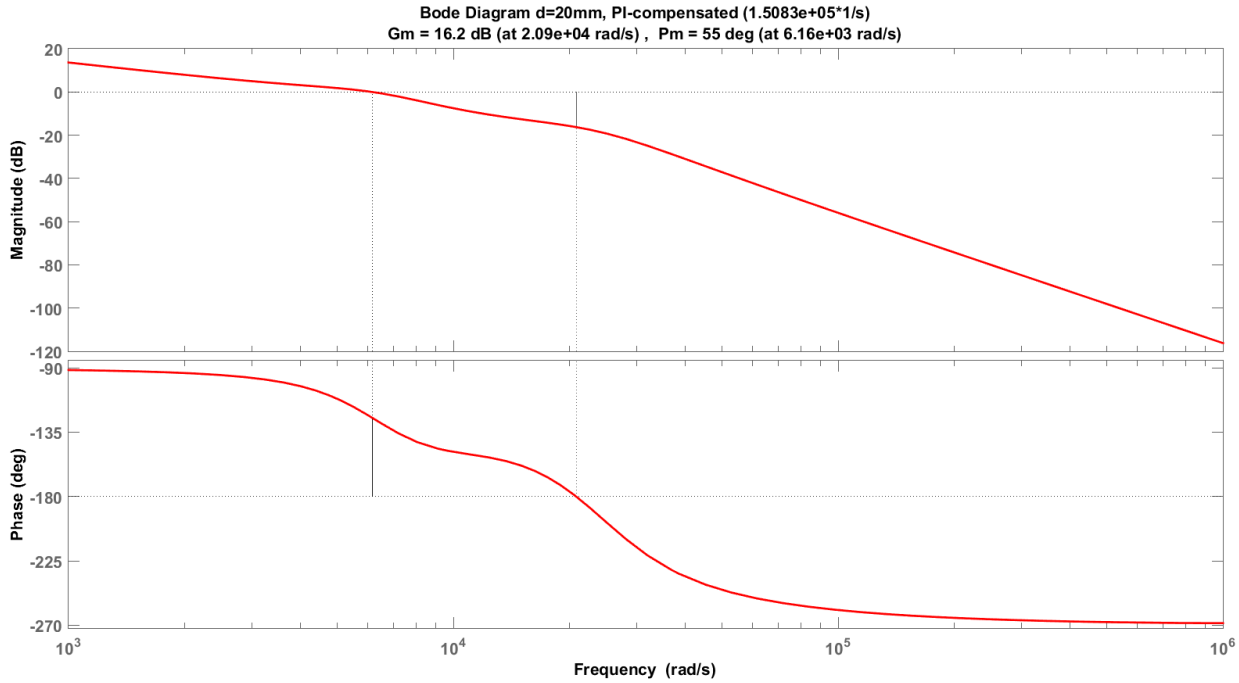

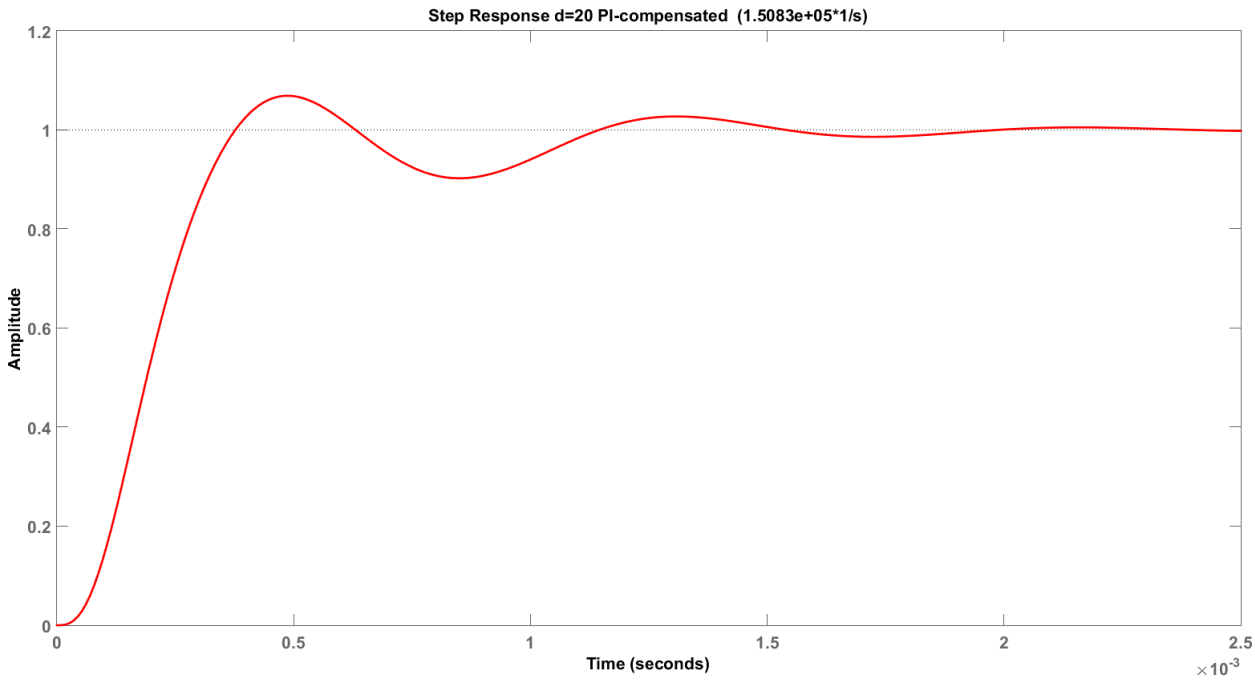
Step Response d=20 PI-compensated (1.5083e+05*1/s)
Amplitude
Time (seconds)
1.2
1
0.8
0.6
0.4
0.2
0
0
0.5
1
1.5
2
2.5
×10-3